

1 **High-time-resolution chemical composition and source apportionment of PM_{2.5} in northern**
2 **Chinese cities: implications for policy**

3 Yong Zhang^{1,2,3}, Jie Tian^{1,2,4}, Qiyuan Wang^{1,2,3,4*}, Lu Qi⁵, Manousos Ioannis Manousakas⁵, Yuemei Han^{1,4}, Weikang
4 Ran^{1,2}, Yele Sun⁶, Huikun Liu^{1,2,4}, Renjian Zhang⁶, Yunfei Wu⁶, Tianqu Cui⁵, Kaspar Rudolf Daellenbach⁵, Jay
5 Gates Slowik⁵, André S. H. Prévôt⁵, Junji Cao^{6*}

6 ¹ State Key Laboratory of Loess and Quaternary Geology, Institute of Earth Environment, Chinese Academy of
7 Sciences, Xi'an 710061, China

8 ² National Observation and Research Station of Regional Ecological Environment Change and Comprehensive
9 Management in the Guanzhong Plain, Shaanxi, Xi'an 710061, China

10 ³ University of Chinese Academy of Sciences, Beijing 100049, China

11 ⁴ Center for Excellence in Quaternary Science and Global Change, Xi'an 710061, China

12 ⁵ Laboratory of Atmospheric Chemistry, Paul Scherrer Institute (PSI), Villigen 5232, Switzerland

13 ⁶ Institute of Atmospheric Physics, Chinese Academy of Sciences, Beijing 100029, China

14 *Correspondence:* wangqy@ieecas.cn (Qiyuan Wang), jjcao@mail.iap.ac.cn (Junji Cao).

15 **Abstract:** Fine particulate matter (PM_{2.5}) pollution is still one of China's most important environmental issues,
16 especially in northern cities during wintertime. In this study, intensive real-time measurement campaigns were
17 conducted in Xi'an, Shijiazhuang, and Beijing to investigate the chemical characteristics and source contributions of
18 PM_{2.5} and explored the formation of heavy pollution for policy implications. The chemical compositions of PM_{2.5} in
19 three cities were all dominated by organic aerosol (OA) and nitrate (NO₃⁻). Results of source apportionment analyzed
20 by hybrid environmental receptor model (HERM) showed that the secondary formation source contributed higher to
21 PM_{2.5} compared to other primary sources. Biomass burning was the dominant primary source in three pilot cities.
22 The contribution of coal combustion to PM_{2.5} is non-negligible in Xi'an and Shijiazhuang but is no longer an
23 important contributor in the capital city of Beijing due to the execution of a strict coal-banning policy. The potential
24 formation mechanisms of secondary aerosol in three cities were further explored by establishing the correlations
25 between the secondary formation source and aerosol liquid water content (ALWC), and O_x (O₃ + NO₂), respectively.
26 The results showed that photochemical oxidation and aqueous-phase reaction were two important pathways of
27 secondary aerosol formation. According to sources variations, air pollution events that occurred in campaigns were
28 classified into three types: biomass combustion dominated, secondary formation source dominated, and a
29 combination of primary and secondary sources. Additionally, this study compared the changes in chemical
30 composition and source contributions of PM_{2.5} in past decades. The results suggested that the clean energy
31 replacements for rural household should be urgently encouraged to reduce the primary source emissions in northern

32 China, and collaborative control on ozone and particulate matter need to be continuously promoted to weaken the
33 atmosphere oxidation capacity for the sake of reducing secondary aerosol formation.

34 **1. Introduction**

35 Fine particulate matter (PM_{2.5}, aerodynamic diameter $\leq 2.5 \mu\text{m}$) is of large concern because of its adverse effects
36 on both natural environment (Kuniyal and Guleria, 2019; Kuo et al., 2013) and human health (Pöschl, 2005; Shen et
37 al., 2021; Zeng and He, 2019). With the soaring economic growth and urbanization in China, PM_{2.5} pollution has
38 been a most serious environmental issue in recent decades (Chan and Yao, 2008; He et al., 2002; Pui et al., 2014;
39 Zhang et al., 2013). The most impressive case is that an extremely severe haze pollution episode occurred in eastern
40 and central China in January 2013 with peak value of PM_{2.5} concentration over $500 \mu\text{g m}^{-3}$. This month had been
41 reported as the haziest month in the past 60 years in Beijing, China (Wang et al., 2014; Huang et al., 2014). Thereafter,
42 aiming to improve air quality, the China central government issued the Air Pollution Prevention and Control Action
43 Plan (APCAP) in September 2013 (http://www.gov.cn/zwggk/2013-09/12/content_2486773.htm, in Chinese), and the
44 Three-year Action Plan to Fight Air Pollution (TAPFAP) in June 2018 (http://www.gov.cn/zhengce/content/2018-07/03/content_5303158.htm, in Chinese). With the implementation of strict pollution controls, air quality in northern
45 China has improved significantly over the past decade (Wang et al., 2020a, 2017; Li et al., 2020). Previous studies
46 show that PM_{2.5} concentration decreased notably in past two decades, and the composition of organic aerosol (OA),
47 black carbon (BC) and sulfate (SO₄²⁻) decreased as well, while the ammonium (NH₄⁺) slightly increased and nitrate
48 (NO₃⁻) increased obviously. In terms of PM_{2.5} sources, contribution of secondary source increased obviously while
49 contribution of industrial emission and coal combustion decreased due to elimination of industries and enterprises
50 with high pollutant emissions, promotion of desulfurization in industrial facilities, replacement of clean energy, and
51 optimization of industrial and energy structures (Lu et al., 2021; Ma et al., 2022; Tao et al., 2017; Wang et al., 2019).
52 However, there is still a significant gap between the PM_{2.5} concentration in northern China and its latest
53 recommendations on air quality guideline ($5 \mu\text{g m}^{-3}$) by the World Health Organization
54 (<https://apps.who.int/iris/bitstream/handle/10665/345329/9789240034228-eng.pdf>, page 78). In addition, severe
55 PM_{2.5} pollutions still frequently occurred in northern China during wintertime (Guo et al., 2021; Li et al., 2017a,
56 2021b). To figure out the causes behind the pollutions and further improve air quality in northern China, it is essential
57 to use online high-time-resolution source apportionment technology to understand the chemical composition and
58 source contribution of PM_{2.5} in those pollution events.
59

60 Recently, more research on measurements of PM_{2.5} and its source apportionments were conducted using online high-
61 time-resolution technologies (Li et al., 2017c; Wang et al., 2021a; Elser et al., 2015). Compared to traditional offline
62 filter-based approach, online methods characterize the short-time variation of PM_{2.5}. It allows for distinguishing the
63 rapid changes and evolutions of chemical components, and is particularly profitable to gain knowledge on the
64 formations of heavy air pollution or episode events (Liu et al., 2016; Ouyang et al., 2019; Zheng et al., 2016; Elser
65 et al., 2015). For instance, Lv et al. (2021) employed a Positive matrix factorization (PMF) model with high-time-
66 resolution online PM_{2.5} data to accurately quantify and distinguish the source distributions in Beijing during two haze
67 episodes in January 2019. Liu et al. (2019) recognized the main drivers of haze event occurred in winter Beijing in
68 2016 according to high-time-resolution source apportionment of PM_{2.5} with multiple models. Furthermore, Wang et
69 al. (2021b) found that vehicle emission contributed most to PM_{2.5} during pollution episodes in downtown Lanzhou
70 based on high-resolution online data source apportionment. Currently, to fully understand and solve heavy pollution
71 events in winter that troubles local governments in northern cities of China (Wang et al., 2022b; Xu et al., 2022; Zhou
72 et al., 2022), more advanced online measurement, and source apportionment is a better choice (Tao et al., 2015). It
73 should be pointed out that previous researches were mainly focused on individual cities, and those results have some
74 limitations in guiding the improvement of air quality in the entire northern region of China. Therefore, it is necessary
75 to conduct comparative research among multiple cities.

76 Considering the differences in geographical location, population, economy, industrial/energy structure, air quality,
77 and depth of air pollution control measures among different cities, three cities in northern China including Beijing,
78 Shijiazhuang and Xi'an were chosen as pilot research subjects. The cities of Beijing and Shijiazhuang are located in
79 the North China Plain, which is one of the most polluted regions in China (Chan and Yao, 2008). Beijing is the capital
80 of China and its air quality has significantly improved under the implementation of the strictest clean air policy since
81 2013 (Li et al., 2021a; Pang et al., 2021; Vu et al., 2019; Zhang et al., 2020). However, the city was still plagued by
82 pollution events in wintertime (Wang et al., 2020b; Yang et al., 2022c; Zhou et al., 2022). Shijiazhuang was
83 recognized as one of the most serious air pollution cities worldwide (Liu et al., 2018b; Huang et al., 2019). Its air
84 quality had also improved under the implementation of the Clean Air Plan, whereas its annual PM_{2.5} concentration
85 was still unable to meet the China's National Ambient Air Quality Standards (NAAQS-II) of 35 $\mu\text{g m}^{-3}$ until 2021
86 (Fig. S1). Xi'an is located in the Fenwei Plain, which is a region that suffered from heavy pollution and was
87 designated as a key region for TAPFAP in 2018 (Cao and Cui, 2021). Compared with Beijing and Shijiazhuang, high-
88 intensity air pollution controls in Xi'an started late due to a lack of financial support. And the annual PM_{2.5}

89 concentration in Xi'an could not meet the NAAQS-II until 2021 as well (Fig. S1). Meanwhile, it is still unclear about
90 the actual causes of the pollution, either topography, meteorological conditions, or local emissions (Chen et al., 2021;
91 Tian et al., 2022; Wang et al., 2015, 2022b). In this study, we conducted intensive real-time observation of PM_{2.5}
92 chemical components in Xi'an, Shijiazhuang, and Beijing during wintertime. The objectives are 1) to determine the
93 characteristics of PM_{2.5} and its chemical components in the three typical northern China cities during wintertime; 2)
94 to quantify the source contribution and explore the potential formation mechanism of secondary aerosols; 3) to
95 explore the unique causes of heavy pollution events in different cities; and 4) to provide suggestions on establishment
96 of efficient policies for air quality continuous improvement. This study provides scientific guidance for developing
97 policy on air quality improvement for northern China cities.

98 **2. Methods**

99 **2.1 Sampling sites and periods**

100 In this study, intensive online measurements of PM_{2.5} were conducted at three pilot cities of Xi'an, Shijiazhuang, and
101 Beijing during wintertime (Fig. 1). The sampling sites in Xi'an and Beijing are located at two Chinese Academy of
102 Sciences (CAS) stations. The one in Xi'an is the Guanzhong Plain Ecological Environment Change and
103 Comprehensive Treatment National Observation and Research Station, Institute of Earth Environment (IEE)
104 (34.24°N, 108.87°E), and another one in Beijing is Tower Branch of the Institute of Atmospheric Physics (IAP)
105 (39.98°N, 116.39°E). Both two sites are surrounded by commercial and residential buildings without intense
106 industrial emissions nearby. Previous studies indicated that these two sites were influenced by biomass and coal
107 burning for heating and cooking during wintertime as well as usual local traffic emissions (Tian et al., 2021; Xu et
108 al., 2021). The sampling site in Shijiazhuang is situated in the courtyard of Hebei Sailhero Environmental Protection
109 High-tech Co., Ltd. (38.04°N, 114.65°E), which is surrounded by pharmaceutical and machine-building industries
110 and close to the streets. The intensive campaigns were continuously conducted for ~1 month in each city (i.e., 12
111 December 12th 2020 to January 7th 2021 in Xi'an, December 20th 2021 to January 24th 2022 in Shijiazhuang, and
112 January 17th 2021 to February 20th 2021 in Beijing).

113 **2.2 Online measurements of PM_{2.5} chemical components**

114 **2.2.1 Organic aerosol and inorganic ions**

115 Concentrations of OA, NO₃⁻, SO₄²⁻, ammonium (NH₄⁺), and chloride (Cl⁻) in PM_{2.5} at a 15-minute time resolution

116 were monitored by a quadrupole aerosol chemical speciation monitor (Q-ACSM, Aerodyne Research Inc., Billerica,
117 Massachusetts, USA) equipped with a PM_{2.5} lens. The detailed operational principles and calibration method of the
118 Q-ACSM are described elsewhere (Ng et al., 2011; Hu et al., 2017). First, the sampled ambient air stream passed
119 through a PM₁₀ impactor inlet and a Nafion[®] dryer (MD-700-24F-3; Perma Pure, Inc., Lakewood, NJ, USA) with a
120 flowrate of 5 L min⁻¹ before entering the Q-ACSM chamber. Then, the pre-treatment particles passed through a 100
121 μm critical orifice at 0.1 L min⁻¹ and were focused into a narrow beam by an aerodynamic intermediate pressure lens.
122 The focused particle beam was flash vaporized by a capture vaporizer (CV) at ~600 °C. The vaporized compounds
123 were then ionized by an electron impactor (EI) ionization source at 70 eV and subsequently analyzed by the
124 quadrupole mass spectrometer.

125 Based on calibration system consists of an atomizer (Model 9302, TSI Inc., Shoreview, MN, USA), a differential
126 mobility analyzer (DMA, TSI model 3080, TSI Inc.), and a condensation particle counter (CPC, TSI model 3772,
127 TSI Inc.), ammonium nitrate (NH₄NO₃) and ammonium sulfate ((NH₄)₂SO₄) aerosol were used for calibration. The
128 raw data of Q-ACSM were analyzed by the ACSM local tool (V1.5.3.5, Aerodyne Research Inc., Billerica,
129 Massachusetts, USA) compiled with Igor Pro 6.37 (Wavemetrics, Lake Oswego, OR, USA). The response factors
130 (RFs) for NO₃⁻ in Xi'an, Shijiazhuang, and Beijing were set as 2.03×10⁻¹¹, and 5.9×10⁻¹¹, 2.20×10⁻¹¹, respectively,
131 and the relative ionization efficiencies (RIEs) for NH₄⁺ and SO₄²⁻ were set as 8.06 and 0.83 in Xi'an, 5.82 and 0.30
132 in Shijiazhuang, 6.31 and 0.38 in Beijing, respectively. Other RIEs for NO₃⁻, OA, and Cl⁻ were set as default values
133 of 1.4, 1.1, and 1.3, respectively (Ng et al., 2011). In addition, the collection efficiency (CE) value of Q-ACSM
134 equipped with a PM_{2.5} lens was recommended as 1 based on laboratory simulation experiments by Xu et al. (2017).
135 Finally, the chemical components monitored by Q-ACSM was corrected by the results of offline filter sampling
136 experiments during the same periods (Fig. S2).

137 **2.2.2 Black carbon**

138 BC concentration in PM_{2.5} was obtained by an Aethalometer (Model AE33, Magee Scientific Inc., Berkeley, CA,
139 USA) with a 1-minute time resolution. The AE33 monitors the light attenuation of seven wavelengths (λ = 370, 470,
140 525, 590, 660, 880, and 940 nm), and the light attenuation at λ = 880 nm was used to calculate BC concentration
141 (Wang et al., 2019; Drinovec et al., 2015). Briefly, the ambient air was first sampled on a filter tape inside the
142 instrument through a PM_{2.5} cyclone (SCC-1.829, BGI Inc., USA) at a flowrate of 5 L min⁻¹. The entering particles
143 were divided into two sample spots on the filter through two channels with different follows. Then the light

144 attenuation transmitted through two parallel spots was detected. For quality accuracies of monitoring, the sampled
145 particles were desiccated with a Nafion[®] dryer (MD-700-24F-3; Perma Pure, Inc., Lakewood, NJ, USA) before
146 entering the AE33. Furthermore, a real-time loading effect compensation algorithm based on two spots measurement
147 was used to eliminate the nonlinear loading effects of the Aethalometer. A detailed description of the Model AE33
148 principle can be found in Drinovec et al. (2015).

149 **2.2.3 Elements**

150 Twenty-four elements, including Si, K, Ca, V, Cr, Mn, Fe, Co, Ni, Cu, Zn, Ga, As, Se, Ag, Cd, Sn, Ba, Au, Hg, Th,
151 Pb, and Pd in PM_{2.5}, were analyzed by a Xact625 Ambient Metals Monitor (Cooper Environmental Services, Tigard,
152 Oregon, USA) with a 1-hour time resolution. Si, K, Ca, Cr, Mn, Fe, Ni, Cu, Zn, As, Se, Ba, and Pb were selected for
153 further analysis in Xi'an and Beijing, while other elements were excluded due to most of their concentration below
154 the method detection limit. In Shijiazhuang, S, Cl, and Ti were analyzed by replacement of Ga, Ag and Au,
155 respectively. Finally, Si, K, Ca, Ti, Cr, Mn, Fe, Ni, Cu, Zn, As, Se, Ba, and Pb were selected for further analysis. The
156 description and detection principles of Xact625 were introduced by Furger et al. (2020) and Rai et al. (2020). In brief,
157 the ambient air stream was firstly sampled on a Teflon filter tape inside the instrument through a PM_{2.5} cyclone inlet
158 at a constant flow rate of 16.7 L min⁻¹, and then the sample was automatically analyzed by nondestructive energy-
159 dispersive X-ray fluorescence (XRF) to determine the mass of the species. For quality control and assurance, the
160 Xact625 performed automatic internal quality control by testing the Pd rod every hour to ensure the stability of the
161 instrument. Energy calibration was performed daily from 00:00 to 00:15 and a range calibration from 00:15 to 00:30
162 local standard time (LST) to monitor any possible shift and instability of the XRF (Liu et al., 2019). During our
163 sampling periods, the concentration of Pd varies within 3 standard deviations (Fig. S3), illustrating the reliable and
164 stable performance of the Xact625.

165 **2.2.4 Complementary data**

166 Online hourly concentrations of PM_{2.5} and gas pollutants (i.e., NO_x, NO₂, CO, SO₂, and O₃) were acquired from the
167 National Air Quality Monitoring Station (<https://air.cnemc.cn:18007/>). Meteorological parameters, including wind
168 speed (WS), wind direction (WD), relative humidity (RH), and temperature (T) were obtained from National
169 Meteorological Station (<http://data.cma.cn/>). The detailed information for complementary data was listed in Table S1.

170 **2.3 Data analysis**

171 2.3.1 PM_{2.5} mass reconstruction

172 Chemical closure was utilized to assess whether chemical compositions can be representative of PM_{2.5}. The sum of
173 OA, NO₃⁻, SO₄²⁻, NH₄⁺, Cl⁻, BC, mineral dust (MD), and trace elements (TE) was considered as the reconstructed
174 PM_{2.5}, where MD and TE were calculated as follows (Chow et al., 2015).

$$175 [\text{MD}] = 2.20 \times [\text{Al}] + 2.49 \times [\text{Si}] + 1.63 \times [\text{Ca}] + 2.42 \times [\text{Fe}] + 1.94 \times [\text{Ti}] \quad (1)$$

$$176 [\text{TE}] = [\text{K}] + [\text{Cr}] + [\text{Mn}] + [\text{Ni}] + [\text{Cu}] + [\text{Zn}] + [\text{As}] + [\text{Se}] + [\text{Ba}] + [\text{Pb}] \quad (2)$$

177 where [] represents the chemical species concentration; [Al] and [Ti] were calculated by the concentration of Ca
178 ([Al] = 4.3 × [Ca] and [Ti] = 0.25 × [Ca]) (Wei et al., 1991). Good correlations between online and reconstructed PM_{2.5}
179 mass (slope = 0.87–1.10, R² = 0.82–0.93) in three pilot cities (Fig. S4) indicated that our measurements could detect
180 major components of PM_{2.5}. The PM_{2.5} concentration used in the following discussion referred to the reconstructed
181 PM_{2.5} concentration.

182 2.3.2 Hybrid environment receptor model

183 Source apportionment of PM_{2.5} was analyzed with a bilinear model named the hybrid environment receptor model
184 (HERM). HERM is developed by the IEECAS and the University of Nevada, Las Vegas (Chen and Cao, 2018). Like
185 other receptor models, the speciation of pollutants at a receptor site can be separated into emission sources and the
186 chemical compositions of the sources. To solve the mass balance of PM_{2.5}, the bilinear HERM in matrix notation is
187 defined as follows

$$188 C_{mn} = \sum_{i=1}^I F_{mi} G_{in} + Q_{mn} \quad (3)$$

189 where C_{mn} is the measured concentration of chemical species m during time n ; F_{mi} is the source profile, that is the
190 fractional quantity of species m in source i emission; G_{in} represents the contribution of source i during time n ; and
191 Q_{mn} is the model residual for species m concentration measured during time n . Based on an iterative conjugate
192 gradient algorithm, the HERM solves G_{in} and unknown F_{mi} by minimizing the Q_{mn} , which is defined as follows.

$$193 Q_{mn} = \sum_{m=1}^M \sum_{n=1}^N \frac{(C_{mn} - \sum_{i=1}^I F_{mi} G_{in})^2}{\sigma_{C_{mn}}^2 + \sum_{i=1}^I (\sigma_{F_{mi}}^2 G_{in}^2 + \delta_{mi} \sigma_{C_{mn}}^2)} \quad (4)$$

194 where M , N , and I are the number of samples, chemical species, and sources, respectively; $\sigma_{F_{mi}}$ represents the error
195 in the variability in the constrained factor profile. δ_{mi} was set to 0 or 1 depending on whether the i^{th} factor profile
196 is constrained or unconstrained, respectively.

197 The HERM input data included the concentration and uncertainty data of chemical species. 19 chemical species in

198 Xi'an and Shijiazhuang and 20 chemical species in Beijing were selected for source apportionment, respectively.
199 Details of selected chemical species and its uncertainty calculation was described in Text S1 in the Supplement. A
200 range from two to ten factors solutions was investigated by HERM with completely unconstrained factor profiles to
201 search for optimal solutions. The detailed diagnostics can be seen in Text S2 in the Supplement. A six-factor solution
202 for Xi'an and Shijiazhuang and an eight-factor solution for Beijing were found to be the optimal solution based on
203 multiple criteria including 1) variations in Q/Q_{exp} which can be used to choose the optimal number of resolved factors,
204 2) physical meaningfulness of distinct factor profiles and explained variation (EV) values of variables, 3) good
205 correlations between sources contribution and external and internal tracers, and 4) agreement between the measured
206 and modeled $\text{PM}_{2.5}$ mass. More detailed information on the final selected factor profiles and contributions is presented
207 in Sect. 3.2.

208 **2.3.3 Aerosol liquid water content**

209 Aerosol liquid water content (ALWC) was calculated by ISORROPIA-II thermodynamic equilibrium model
210 (<http://isorrophia.eas.gatech.edu/>) based on data of $\text{PM}_{2.5}$ chemical species (including NO_3^- , SO_4^{2-} , NH_4^+ , and Cl^-) and
211 meteorological parameters including relative humidity (RH) and temperature (T), more model information can be
212 found in Fountoukis and Nenes (2007). It should be noted that the ISORROPIA-II model does not consider the
213 contribution of the organic, as inorganic aerosols are the most hygroscopic species and dominant contributor to
214 ALWC (Huang et al., 2020).

215 **3. Results and discussion**

216 **3.1 Characteristics of $\text{PM}_{2.5}$ and its chemical components**

217 Figure 1 illustrates the mass composition of $\text{PM}_{2.5}$ in three pilot cities during the sampling periods, and their
218 concentrations levels are summarized in Table S4. The average $\text{PM}_{2.5}$ concentrations in Xi'an, Beijing, and
219 Shijiazhuang were $77 \pm 47 \mu\text{g m}^{-3}$, $64 \pm 57 \mu\text{g m}^{-3}$, and $60 \pm 39 \mu\text{g m}^{-3}$, respectively. It is noted that the average $\text{PM}_{2.5}$
220 concentrations in Xi'an, Beijing, and Shijiazhuang did not meet the second level of the NAAQS, indicating that it is
221 necessary to establish more particular and efficient pollution reduction measures. As shown in Fig. 1, the chemical
222 compositions of $\text{PM}_{2.5}$ were similar in Beijing and Shijiazhuang (Fig. 1b and c) which was mainly composed of OA
223 (26.9–34.2%), followed by NO_3^- (23.6–26.5%), SO_4^{2-} (11.8–15.0%), NH_4^+ (11.8–14.8%), MD (7.4–10.1%), BC (2.9–
224 6.5%), and Cl^- (1.1–4.8%). However, in Xi'an, MD contributed in comparison more to $\text{PM}_{2.5}$ (17.3%), while SO_4^{2-}

225 had a smaller contribution (6.8%). This could be explained by more construction activities and MD transport from
226 the Loess Plateau to Xi'an (Long et al., 2016; Yan et al., 2015). Meanwhile, the lowest sulfur oxidation ratio (SOR)
227 was observed in Xi'an (0.18 ± 0.08 , see Table S5), indicating weak efficiency of the second generation of SO_4^{2-} . The
228 sum of SO_4^{2-} , NO_3^- and NH_4^+ accounted for 39.0–53.0% of $\text{PM}_{2.5}$ in three pilot cities, highlighting the importance of
229 the secondary inorganic components in northern China. In addition, the fractions of BC, Cl^- , and TE in $\text{PM}_{2.5}$ were
230 lower in Beijing than those in the other two cities, which can be explained by the stricter local control policies on
231 solid fuels combustion and tightening the industrial emission standards in and near the capital city of China (Li et al.,
232 2021a; Pang et al., 2021).

233 To better understanding the impact of the chemical components, the mass fraction of each component was plotted as
234 a function of the $\text{PM}_{2.5}$ mass concentration (Fig. 2a–c). The two dominant components of $\text{PM}_{2.5}$ were OA (25.7–
235 38.0%) and MD (19.9–37.1%) while the $\text{PM}_{2.5}$ concentrations were below $40 \mu\text{g m}^{-3}$. The fraction of OA in $\text{PM}_{2.5}$ was
236 the highest in Shijiazhuang and Beijing, while MD contributed most to $\text{PM}_{2.5}$ in Xi'an. This is potentially related to
237 more emissions and higher backgrounds of local dust. With increases of the $\text{PM}_{2.5}$ mass concentration, the fractions
238 of chemical components in Xi'an and Shijiazhuang changed notably. The fractions of OA and NO_3^- increased the most
239 and reached the peaks of 40.1% and 28.7%, respectively, when the $\text{PM}_{2.5}$ concentration reached $\sim 196 \mu\text{g m}^{-3}$ in Xi'an.
240 On the contrary, NO_3^- and SO_4^{2-} were two dominant drivers of increasing $\text{PM}_{2.5}$ concentrations in Shijiazhuang,
241 showing peak contributions of 32.5% and 18.7%, respectively, when the $\text{PM}_{2.5}$ concentration was over $100 \mu\text{g m}^{-3}$.
242 Compared to Xi'an and Shijiazhuang, Beijing had relatively stable fractions of each chemical component with
243 increasing $\text{PM}_{2.5}$ concentrations. Particularly, the fractions of OA and NO_3^- contributed dominantly with averages of
244 $33.3 \pm 3.0\%$ and $25.3 \pm 2.5\%$, respectively, when the $\text{PM}_{2.5} > 40 \mu\text{g m}^{-3}$.

245 **3.2 Source apportionment of $\text{PM}_{2.5}$**

246 Six potential sources, including biomass burning, fugitive dust, industrial emission, coal combustion, vehicle
247 emission, and secondary formation source, were resolved by the HERM analysis. In Beijing, secondary formation
248 source was furtherly divided into secondary nitrate plus OA and secondary sulfate plus OA. A special pollution source
249 of firework was separated due to the Chinese Spring Festival (from New Year's Eve to January 3rd in the lunar
250 calendar). Figures S6–S8 present the sources profiles and contributions in Xi'an, Shijiazhuang, and Beijing,
251 respectively. Biomass burning features high Explained Variation (EV) for the two tracers Cl^- (33–58%) and K (30–
252 44%) in the three cities (Ni et al., 2017; Zhao et al., 2021). The fugitive dust is characterized by high EV values for

253 Si (60–90%) and Ca (34–54%), which are the dominant chemical species in the fugitive dust profiles in northern
254 China (Shen et al., 2016; Zhao et al., 2006). The fractions of industrial emission vary among the cities, showing high
255 EV for Ni (55% and 87%) and Cr (25% and 70%) in Xi'an and Shijiazhuang, and high EV for Cr (26%), Mn (40%),
256 and Pb (27%) in Beijing. Ni is possibly emitted from the semiconductor industry (Simka et al., 2005). Cr, Mn, and
257 Pb could originate from the steel manufacturing and incinerator fly ash (Duan and Tan, 2013; Ledoux et al., 2017).
258 Coal combustion is characterized by high EV values for As (38–75%), Se (40–50%), and Pb (31–57%). These
259 elements are enriched in coals, which are reliable indicators of coal combustion (Tian et al., 2013; Xu et al., 2012).
260 The vehicle non-exhaust emissions could be identified by the elements Ba, Cu, Ca, Fe, and Mn. Cu and Ba can be
261 released from brake and tire wear of vehicles (Adachi and Tainosho, 2004; Thorpe and Harrison, 2008). Moreover,
262 Fe and Mn could be emitted from the combustion of lubricating oil and fuel additives (Ålander et al., 2005; Lewis et
263 al., 2003). Relatively high EV values for Ba (68%), Cu (36%), and Ca (35%) are seen in Xi'an, significantly high
264 EV values of Mn (68%), Fe (65%), Cu (53%), and Ba (80%) are characterized in Shijiazhang and relatively high EV
265 values of Fe (34%) and Cu (39%) are featured in Beijing, respectively. Moreover, moderate EV values for BC (18–
266 27%) and OA (13–22%) are commonly regarded as contributions of vehicles engine exhaust, while the temporal
267 variations of VE are well correlated with gaseous NO_x or NO₂ in three cities ($R^2 = 0.45–0.78$), which is the good
268 tracer of traffic-related emissions (Huang et al., 2017; Li et al., 2017b). The secondary sources resolved by HERM
269 are different among the three cities. In Xi'an and Shijiazhuang, this factor are characterized by high EV values for
270 SO₄²⁻ (62–75%), NO₃⁻ (55–53%), NH₄⁺ (60–56%) and a medium EV value for OA (23–29%), which showed good
271 correlations with SO₄²⁻ ($R^2 = 0.85–0.90$) and NO₃⁻ ($R^2 = 0.85–0.92$) (Dai et al., 2020; Tian et al., 2022). In addition,
272 The OA concentration in this factor was calculated by EV value of OA, which was close to the secondary OA (SOA)
273 concentration estimated by BC-trace method (see Text S3 and Table S6). This means that SOA was mixed in this
274 factor, therefore, this factor was identified as secondary formation source. In Beijing, two secondary sources were
275 resolved. The first one was characterized by high EV value for NO₃⁻(58%), NH₄⁺ (42%) and medium values for OA
276 (21%), another one was characterized by high EV value for SO₄²⁻(58%), and medium values for OA (16%), NH₄⁺
277 (30%). The OA concentration in those two factors was also comparable to that estimated by BC-trace method (see
278 Text S3). So, those two sources were identified as secondary nitrate plus OA and secondary sulfate plus OA,
279 respectively. The combination of secondary nitrate plus OA and secondary sulfate plus OA is equivalent to the
280 secondary formation source for next discussion. Additionally, the source of firework emission is characterized by
281 high EV values of Ba (83%), Cu (45%), and K (38%), which are recognized as common indication in fireworks (Rai
282 et al., 2020; Tian et al., 2014).

283 The modeled PM_{2.5} mass was well correlated with the reconstructed PM_{2.5} mass ($R^2 = 0.99$, slope = 0.90–1.01, Fig.
284 S10) in three pilot cities, indicating the established models are reasonable. As shown in Fig. 1d and e, the contributions
285 of primary sources (i.e., the sum of biomass burning, fugitive dust, industrial emission, coal combustion, and vehicle
286 emission) in PM_{2.5} were significantly higher than those of the secondary formation source in Xi'an and Shijiazhuang,
287 indicating the PM_{2.5} in these two cities are mainly influenced by the primary source emissions during wintertime.
288 Particularly, biomass burning and coal combustion were two dominant contributors to PM_{2.5} with contributions of
289 24.6% and 15.1%, respectively, in Xi'an; and 24.4% and 16.0%, respectively, in Shijiazhuang. These suggest that
290 controls of solid fuel combustion are critical to reducing PM_{2.5} pollution in these cities. In contrast, the contribution
291 of secondary formation source to PM_{2.5} in Beijing was highly dominant (> 50%), potentially attributed to strict control
292 of primary emissions under the execution of a series of pollution control policies (Lv et al., 2016; Pang et al., 2021),
293 and more regional transportation of secondary pollutants (Liu et al., 2019; Wang and Zhao, 2018). Among the primary
294 sources, the contributions of biomass burning and vehicle emission were only 18.4% and 11.3%, respectively, further
295 reflecting the benefits of reductions of all primary emissions. Due to the Chinese Spring Festival, the contribution of
296 firework (7.9%) to PM_{2.5} ranked second in primary sources (Fig. S11). Which indicates more refined control schemes
297 need to be encouraged to deal with such special event in the future. It should be noted that contribution of fugitive
298 dust was all lower than fraction of mineral dust in the three pilot cities (Fig. 1). This is because fugitive dust defined
299 here mainly refers road and construction dust emission. While mineral dust represents material assumed oxides of
300 mineral elements such as Al, Si, Ca, Ti and Fe (Chow et al., 2015). These mineral elements in PM_{2.5} comes from
301 more emission sectors including industry, crust, and transportation, construction, combustion (Liu et al., 2018a; Lu
302 et al., 2014; Pant and Harrison, 2013; Shen et al., 2016).

303 Figures 2d–f shows variations of source contribution with increases in PM_{2.5} mass concentrations in three pilot cities.
304 The most two dominant sources were secondary formation source (32.1%) and fugitive dust (31.4%) in Xi'an, coal
305 combustion (24.9%) and vehicle emission (21.3%) in Shijiazhuang, and secondary formation source (24.3%) and
306 fugitive dust (23.8%) in Beijing, when the PM_{2.5} mass concentration <40 $\mu\text{g m}^{-3}$. In Xi'an, when the PM_{2.5} mass
307 concentrations exceeded 180 $\mu\text{g m}^{-3}$, the contribution of biomass burning raised mostly and reached the peak of
308 38.4%, demonstrating that biomass burning plays an important role in worsening of air quality in Xi'an. On the
309 contrary, the contributions of secondary formation source increased mostly in comparison to other sources in
310 Shijiazhuang and Beijing, indicating the PM_{2.5} pollution was mainly dominated by the secondary aerosol formations
311 during the wintertime. And the peak contributions of secondary nitrate and sulfate were 66.5% and 74.7% while the

312 PM_{2.5} mass concentration increased to 113 $\mu\text{g m}^{-3}$ and 223 $\mu\text{g m}^{-3}$ in Shijiazhuang and Beijing, respectively.

313 **3.3 Formation of secondary aerosols**

314 Using the high-time-resolution data, we further explored the possible formation mechanisms of secondary formation
315 source. The concentration of secondary formation source is standardized by dividing background corrected CO (ΔCO)
316 to weaken impact of planetary boundary layer height (PBLH) (DeCarlo et al., 2010). In this study, ΔCO is defined as
317 the 1.25th percentile of CO concentration during the campaign, which are 0.17, 0.15, and 0.16 ppm in Xi'an,
318 Shijiazhuang, and Beijing, respectively. O_x ($\text{NO}_2 + \text{O}_3$) is an indicator of the photochemical oxidation degree (Wood
319 et al., 2010). The function between secondary formation source/ ΔCO ratio and O_x during the daytime (i.e., 08:00–
320 17:00 LST) (Fig. S12) was plotted to explain the effect of photochemical oxidations in three pilot cities. As shown
321 in Fig. 3, good linear correlations of secondary formation source/ ΔCO and O_x ($R^2 = 0.83\text{--}0.99$) suggest that
322 photochemical oxidations play an important role in the formation of secondary aerosol during the daytime. Compared
323 to the low-level O_x , formation of secondary aerosol significantly enhanced at high-level O_x (>50 ppb) in Xi'an and
324 Beijing, characterized by larger slopes of 17.2 and 38.9, respectively (Fig. 3a and c). Furthermore, the highest
325 atmospheric oxidation capacity was found in Beijing, inferring by the highest fraction of O_3 to O_x . This is consistent
326 with the highest contribution of secondary formation source to PM_{2.5} in Beijing during the daytime (Fig. S13a–c).

327 The aqueous-phase reaction is another important pathway for secondary aerosol formation in the atmosphere (Wang
328 et al., 2018; Xue et al., 2014). ALWC is considered an indicator of an aqueous-phase reaction (Ervens et al., 2011).
329 Considering that the aqueous-phase reaction occurs both during the daytime and nighttime characterized by good
330 correlations between secondary formation source/ ΔCO and ALWC ($R^2 = 0.81\text{--}0.98$, Fig. S14). The correlations of
331 secondary formation source/ ΔCO ratio and ALWC during all sampling periods were re-established in three pilot cities
332 to assess the implications of aqueous-phase chemistry for secondary aerosol production. As shown in Fig. 4, the
333 secondary formation source/ ΔCO showed a significant linear correlation to ALWC ($R^2 = 0.92\text{--}0.99$) when $\text{RH} < 80\%$,
334 indicating an obvious effect of aqueous-phase reaction on the secondary aerosol formation during the sampling
335 periods. However, when $\text{RH} > 80\%$, the secondary formation source/ ΔCO showed no notable increase with ALWC
336 in Shijiazhuang (Fig. 4b), whereas a tiny increase with ALWC in Beijing (Fig. 4c). The higher ALWC at $\text{RH} > 80\%$
337 probably inhibits secondary aerosol formation due to the decrease in aerosol acidity (Huang et al., 2019; Meng et al.,
338 2014). Khan et al. (2008) found that NO_3 radicals can rapidly generate from the reaction between NO_2 and O_3 with
339 unsaturated organic species during nighttime. The value of $\text{O}_3 \times \text{NO}_2$ can thus represent its production reaction rate or

340 be used as a proxy for the NO₃ radical. The highest NO₃ radical production rate was found in Beijing, followed by
341 Xi'an and Shijiazhuang, when RH<80%. This could be used to explain the highest contribution of secondary
342 formation source to PM_{2.5} in Beijing during the daytime and nighttime (Fig. S13). Moreover, the results showed that
343 both photochemical oxidation and aqueous-phase reaction play more important roles in Beijing, where the primary
344 sources have been better controlled. This reflects that pollution control policies need to be focused on the suppression
345 of secondary formations.

346 **3.4 Elaborations of different episode cases**

347 During the sampling periods, the concentration of PM_{2.5} and its chemical components accumulated within a short
348 period in a few cases (Fig.S15a-c). We define such a rapid rise in PM_{2.5} mass concentration as a pollution episode.
349 As shown in Table 1, meteorological conditions, the concentration levels of gaseous pollutants, chemical
350 compositions, and source contributions of PM_{2.5} during pollution episodes in three pilot cities are summarized. The
351 episodes were accompanied by low wind speed (< 2 m s⁻¹), leading to weak dispersions of fresh emissions and
352 accumulated pollutants (Chen et al., 2020b). OA and NO₃⁻ were the two dominant chemical components in PM_{2.5}
353 during all pollution episode cases with fractions of 26–40% and 23–32%, respectively. Their high abundances could
354 be explained by the significant reduction of SO₂ emissions because of the prohibiting of burning bulk coals and
355 executing the “Coal-to-Natural Gas” policy in recent years (Meng et al., 2022). In this study, eight pollution episodes
356 (donated as EP1-EP8) were classified into three types: The first type was dominated by biomass burning (30–40%)
357 (EP1, EP4, and EP8). The second type was dominated by secondary formation source (61–70%) (EP5, EP6, and EP7).
358 The two remaining pollution episodes were mutually contributed by both primary and secondary sources (EP2 and
359 EP3), in which secondary formation source (34–39%) and biomass burning (23–24%) were the two dominant
360 contributors to PM_{2.5}.

361 To gain insights into the process of pollution episodes, three typical pollution events were chosen for detailed
362 discussion (i.e., EP2 in Xi'an, EP4 in Shijiazhuang, and EP7 in Beijing) based on the validity and integrity of the
363 data and the representativeness of the selected pollution events. The two-stage evolution was distinguished for EP4
364 as an example of the first type of episode (Fig. S16). At Stage 1, the PM_{2.5} mass concentrations rapidly increased
365 from 7 to 82 μg m⁻³ under stable weather conditions inferring by low wind speed (1.8±0.8 m s⁻¹, Fig. S16b), in which
366 the concentrations (fractions) of biomass burning increased from 0.6 μg m⁻³ (7%) to 36.7 μg m⁻³ (55%) due to heating
367 activities during nighttime. Meanwhile, the chemical composition was relatively stable and dominated by OA (31±5%)

368 and NO_3^- (21±5%). At Stage 2, the $\text{PM}_{2.5}$ mass concentration continuously increased to $105 \mu\text{g m}^{-3}$ in a few hours
369 along with the most notable abundance of the source of secondary formation source, which concentration
370 (contribution) rapidly increased from $2.3 \mu\text{g m}^{-3}$ (4%) to $54.4 \mu\text{g m}^{-3}$ (52%) (Fig. S16g and h). This is due to the
371 aqueous-phase reactions effect inferring by the rapid increase in ALWC (from $16 \mu\text{g m}^{-3}$ to $78 \mu\text{g m}^{-3}$, Fig. S16c) and
372 RH (from 51% to 79%, Fig. S16a).

373 In contrast, a three-stage evolution was discriminated for the second type of episode, using EP7 as an example (Fig.
374 S17). At Stage 1, the $\text{PM}_{2.5}$ concentration gradually increased from 11 to $30 \mu\text{g m}^{-3}$, as well as NO_2 (from 15 to 59
375 $\mu\text{g m}^{-3}$, Fig. S17d) due to the boosts of the predominant contributions of vehicle emission and biomass burning (Fig.
376 S17g and h). In the meantime, the contribution of coal combustion also slowly increased along with SO_2 (Fig. S17d
377 and h). At Stage 2, under the lowest average wind speed in the study period ($0.7 \pm 0.4 \text{ m s}^{-1}$, Fig. S17b), the $\text{PM}_{2.5}$
378 mass concentrations moderately increased from 30 to $91 \mu\text{g m}^{-3}$ with relatively stable chemical composition and
379 source contribution (Fig. S17f and h). Compared to Stage 1, the fractions of NO_3^- increased mostly from $9 \pm 3\%$ to
380 $23 \pm 3\%$, this is probably influenced by photochemical oxidations inferring by relative high O_x and NO_2 concentration
381 (Fig. S17c and d). At Stage 3, the $\text{PM}_{2.5}$ mass concentration rapidly rose to $142 \mu\text{g m}^{-3}$ and then remained stable.
382 Furthermore, the greatest increase of sources concentrations (contribution) was secondary formation source from
383 $18.9 \mu\text{g m}^{-3}$ (48%) to $120.6 \mu\text{g m}^{-3}$ (80%). This might be due to the occurrence of an aqueous-phase reaction, which
384 was indicated by the elevation of RH and ALWC (Fig. S17a and c).

385 Figure S16 illustrates the third type of episode using EP2 as an example, in which a four-stages evolution was resolved.
386 At Stage 1, the $\text{PM}_{2.5}$ mass concentration ($14 \pm 3 \mu\text{g m}^{-3}$) was relatively low and dominated by the contributions of
387 secondary formation source ($43 \pm 17\%$) and fugitive dust ($24 \pm 8\%$), as well as MD ($28 \pm 7\%$) and OA ($26 \pm 7\%$). At
388 Stage 2, the $\text{PM}_{2.5}$ mass concentrations promptly increased from 21 to $82 \mu\text{g m}^{-3}$, with the two dominant chemical
389 components of OA ($21.7 \mu\text{g m}^{-3}$) and NO_3^- ($17.1 \mu\text{g m}^{-3}$). The $\text{PM}_{2.5}$ increases can be also attributed to the raise of
390 secondary formation source ($25.3 \mu\text{g m}^{-3}$) and biomass burning ($14.4 \mu\text{g m}^{-3}$). The enhancement of secondary aerosol
391 was probably generated through the aqueous-phase reaction evidenced by the increase of ALWC and NO_2 (Fig. S18c
392 and d). At Stage 3, $\text{PM}_{2.5}$ mass continuously increased to $139 \mu\text{g m}^{-3}$ with a dominant increase of primary sources
393 emission including biomass burning ($29.0 \mu\text{g m}^{-3}$), vehicle emission ($21.5 \mu\text{g m}^{-3}$) and coal combustion ($16.5 \mu\text{g m}^{-3}$)
394 along with the increases of SO_2 and NO_2 as well (Fig. S18d). The three primary sources contributed >60% of the
395 total resolved sources. Meanwhile, the secondary formation source also increased slowly through aqueous-phase

396 reaction inferring by increase of ALWC (Fig. S18c). At the final Stage 4, the PM_{2.5} mass concentration maintained
397 relatively stable with an average of 142±11 μg m⁻³, dominated by secondary formation source (34±6%) and biomass
398 burning (28±6%); and chemical components of OA (36±4%) and NO₃⁻ (25±1%).

399 In summary, the pollution events occurred in Xi'an was mainly derived by stronger emissions of primary sources
400 under adverse meteorological conditions, even though the aqueous-phase reaction also contribute to secondary
401 aerosol formation. In contrast, pollution events occurred in Shijiazhuang and Beijing were mainly influenced by
402 formation of secondary aerosols through both of aqueous-phase reaction and photochemical oxidation. What's more,
403 aqueous-phase reaction plays a more important role than photochemical oxidation. Hence, to further improve the air
404 quality in the north of China, primary source emissions should be prioritized for control in the northwest region, with
405 a focus on biomass burning and coal combustion. In the North China Plain, the priority should be given to reduce
406 emissions of the precursors from secondary sources, with a focus on NO_x and volatile organic compounds (VOCs).

407 **3.5 Policy implications**

408 In past decades, the air quality in China improved notably under the implementation of air pollution control policies
409 including APCAP and TAPFAP. The PM_{2.5} mass in Xi'an, Shijiazhuang and Beijing were the lowest during campaigns
410 compared with those in last decades (Table S7). The variations of the chemical composition and the source
411 contribution of PM_{2.5} in the three pilot cities are displayed in Fig. 5. As shown, the dominant chemical components
412 of PM_{2.5} changed from OA and SO₄²⁻, to OA and NO₃⁻ (Fig. 5a–c). This could be attributed to the reduction in coal
413 consumption due to clean energy replacement and the increase of vehicle ownership, which lead a decrease of the
414 SO₂ and an increase of NO₂ (Wang et al., 2013). Since the atmospheric oxidation reaction (i.e., aqueous-phase reaction
415 and photochemical oxidation) of the precursors (i.e., NO₂, VOCs) is the primary source for the OA and NO₃⁻ in the
416 atmosphere (Feng et al., 2018; Li et al., 2022; Tao et al., 2016; Yang et al., 2022b; Ziemann and Atkinson, 2012), and
417 it is impossible to avoid, thus, the precursors of OA and NO₃⁻ should be reduced from the combustion and
418 transportation sectors (Fermo et al., 2021; Liu et al., 2022; Wang et al., 2021c; Zhang et al., 2019). In addition, the
419 fraction of NH₄⁺ in PM_{2.5} increased with an alarming rate. This is coincidentally in a similar trend of NH₃. Studies
420 have reported that controls of NH₄⁺ is more effective than that of NO_x in the reduction of PM_{2.5} mass concentrations
421 (Gu et al., 2021; Zheng et al., 2022). Therefore, collaborative control measures for the emissions of precursors
422 including NO_x, VOCs, and NH₃ are necessary.

423 As shown Table S8 and Fig. 5d-f, coal combustion decreased remarkably due to the coal-related policies
424 implementation including the strength of emissions standards for coal-fired power plants, the change of energy
425 sources from coal to natural gas in some industrials, and the coal burning was forbidden in the main urban areas
426 (Shen, 2016; Yang and Teng, 2018). The similar trend was also founded in the results of PM_{2.5} source apportionment
427 in Beijing released by Beijing Municipal Ecology and Environment Bureau (Fig. S19). Meanwhile, the
428 contribution of industrial emission and vehicle emission decreased slightly because of the improvement of industrial
429 emission standards (He et al., 2020; Wang et al., 2020a) and the traffic-related policy implementation such as the
430 strength of vehicle emission standards, improvement of fuel quality, and elimination of high-emission-vehicles. This
431 resulted in the reduction of the precursor gases and PM_{2.5} from vehicles (Feng et al., 2021; Fontaras et al., 2012; Jin
432 et al., 2012). However, the emission of biomass burning did not show a significant reduction in recent years, and its
433 contribution increased from 9% in 2014 to 25% in 2020 (Xi'an), from 3% in 2015 to 24% in 2022 (Shijiazhuang),
434 and from 6% in 2013 to 18% in 2021 (Beijing) (Fig. 5d-f). This is likely because biomass burning is an open source,
435 which makes it more difficult to control compare with other primary sources. Biomass used for residential heating in
436 rural areas is still frequently occurred (Ren, 2021; Tian et al., 2022; Yang et al., 2022a; Zhang et al., 2017). Hence,
437 the clean energy revolution should be promoted urgently especially in the entire regions in northwest China. Moreover,
438 the contributions of secondary formation source increased, it is potentially explained by the high reduction rate of
439 primary emissions and the improvement of atmospheric oxidation capacity (Chen et al., 2020a; Feng et al., 2020).
440 Therefore, more control measures should focus on weakening the atmospheric oxidation capacity, such as reduction
441 of O₃ formation, to reduce the formation of secondary pollutants which are now identified as the most critical drivers
442 of pollution. Considering those factors, it is also important to promote the mitigation of *both* PM_{2.5} and O₃.

443 **4. Conclusion**

444 The intensive real-time measurement campaigns about PM_{2.5} chemical components were conducted in Xi'an,
445 Shijiazhuang, and Beijing during the wintertime respectively. Chemical compositions of PM_{2.5} in the three cities were
446 all dominated by OA (26.9–34.2%) and NO₃⁻ (23.6–26.5%). Six sources of PM_{2.5} in Xi'an and Shijiazhuang were
447 resolved by HERM and their contributions were similar, with a descending order of secondary formation source
448 (32.2–37.6%), biomass burning (24.4–24.6 %), coal combustion (15.1–16.0%), vehicle emission (12.2–12.5 %),
449 industrial emission (5.5–7.7%) and fugitive dust (4.4–7.8%). However, the secondary nitrate (29.0%) and the
450 secondary sulfate (23.0%) were separately resolved and relatively more important in Beijing. In addition, the
451 contribution of firework (7.9%) to PM_{2.5} was found during the Chinese Spring Festival.

452 The possible formation mechanism of secondary formation source in three pilot cities was explored. The results
453 showed that secondary aerosols were generated by both photochemical oxidation and aqueous-phase reaction.
454 Meanwhile, the formation rate of secondary aerosols in Beijing was higher than that in Xi'an and Shijiazhuang.
455 Furthermore, the eight pollution episodes within the sampling periods were categorized three types and characterized
456 respectively. The dominant chemical compositions of PM_{2.5} were OA (26–40%) and NO₃⁻ (23–32%) during all
457 pollution episodes. Furthermore, secondary formation source and biomass burning were two major derivors of the
458 pollution.

459 The dominant chemical components of PM_{2.5} in pilot cities have changed from OA and SO₄²⁻ to OA and NO₃⁻ under
460 the implementation of a clean air plan in past decades. This indicates that reduction of precursors including NO₂ and
461 VOCs should be a key task in the future. In addition, the contribution of biomass burning increased, especially in
462 Xi'an. This indicates that clean energy for heating activities in rural areas in northwest China is still insufficient.
463 Furthermore, to weaken the atmospheric oxidation capacity for reducing the contribution of secondary formation
464 source, it is necessary to promote the collaborative control on ozone and particulate matter.

465 *Data availability.* Data used to support the findings in this study are archived at the Institute of Earth Environment,
466 Chinese Academy of Sciences, and are publicly available at <https://doi.org/10.5281/zenodo.8106655>.

467 *Competing interest.* The authors declare that they have no conflict of interest.

468 *Author contributions.* QW, YH, JC designed the campaigns. WR and YZ conducted the field measurements. YZ, JT,
469 HL, LQ and TC performed data analysis and interpretation. MM, KRD, JGS and ASHP were involved supervision
470 and review. YZ wrote the paper with contributions from all co-authors.

471 *Acknowledgments.* The authors are grateful to the staff from Guanzhong Plain, Eco-environmental Change and
472 Comprehensive Treatment, National Observation and Research Station; Tower Branch of Institute of Atmospheric
473 Physics, Chinese Academy Sciences; and Hebei Sailhero Environmental Protection High-tech Co., Ltd. for their
474 assistance with field sampling.

475 *Financial support.* This work was financially supported by the Sino-Swiss Cooperation on Air Pollution for Better
476 Air (7F-09802.01.02) from the Swiss Agency for Development and Cooperation (SDC), the National Key R&D
477 Program of China (2022YFF0802501), and the Youth Innovation Promotion Association of the Chinese Academy of

478 Sciences (2019402). Natural Science Basic Research Program of Shaanxi (2022JQ-267)

479

480

References:

- 481 Adachi, K. and Tainosho, Y.: Characterization of heavy metal particles embedded in tire dust, *Environ. Int.*, 30, 1009–
482 1017, <https://doi.org/10.1016/j.envint.2004.04.004>, 2004.
- 483 Ålander, T., Antikainen, E., Raunemaa, T., Elonen, E., Rautiola, A., and Torkkell, K.: Particle emissions from a small
484 Two-Stroke engine: Effects of fuel, lubricating oil, and exhaust aftertreatment on particle characteristics, *Aerosol*
485 *Sci. Technol.*, 39, 151–161, <https://doi.org/10.1080/027868290910224>, 2005.
- 486 Cao, J. J. and Cui, L.: Current status, characteristics and causes of particulate air pollution in the Fenwei Plain, China:
487 A Review, *J. Geophys. Res-Atmos.*, 126, <https://doi.org/10.1029/2020JD034472>, 2021.
- 488 Chan, C. K. and Yao, X.: Air pollution in mega cities in China, *Atmos. Environ.*, 42, 1–42,
489 <https://doi.org/10.1016/j.atmosenv.2007.09.003>, 2008.
- 490 Chen, L.-W. A. and Cao, J. J.: PM_{2.5} source apportionment using a hybrid environmental receptor model, *Environ.*
491 *Sci. Technol.*, 52, 6357–6369, <https://doi.org/10.1021/acs.est.8b00131>, 2018.
- 492 Chen, Q., Hua, X., Li, J. W., Chang, T., and Wang, Y.: Diurnal evolutions and sources of water-soluble chromophoric
493 aerosols over Xi'an during haze event, in Northwest China, *Sci. Total Environ.*, 786, 147412,
494 <https://doi.org/10.1016/j.scitotenv.2021.147412>, 2021.
- 495 Chen, S., Wang, H., Lu, K., Zeng, L., Hu, M., and Zhang, Y.: The trend of surface ozone in Beijing from 2013 to
496 2019: Indications of the persisting strong atmospheric oxidation capacity, *Atmos. Environ.*, 242, 117801,
497 <https://doi.org/10.1016/j.atmosenv.2020.117801>, 2020a.
- 498 Chen, Z., Chen, D., Zhao, C., Kwan, M., Cai, J., Zhuang, Y., Zhao, B., Wang, X., Chen, B., Yang, J., Li, R., He, B.,
499 Gao, B., Wang, K., and Xu, B.: Influence of meteorological conditions on PM_{2.5} concentrations across China: A
500 review of methodology and mechanism, *Environ. Int.*, 139, 105558,
501 <https://doi.org/10.1016/j.envint.2020.105558>, 2020b.
- 502 Chow, J. C., Lowenthal, D. H., Chen, L.-W. A., Wang, X., and Watson, J. G.: Mass reconstruction methods for PM_{2.5}:
503 a review, *Air Qual. Atmos. Health*, 8, 243–263, <https://doi.org/10.1007/s11869-015-0338-3>, 2015.
- 504 Dai, Q., Liu, B., Bi, X., Wu, J., Liang, D., Zhang, Y., Feng, Y., and Hopke, P. K.: Dispersion normalized PMF provides
505 insights into the significant changes in source contributions to PM_{2.5} after the COVID-19 outbreak, *Environ. Sci.*
506 *Technol.*, 54, 9917–9927, <https://doi.org/10.1021/acs.est.0c02776>, 2020.
- 507 DeCarlo, P. F., Ulbrich, I. M., Crouse, J., de Foy, B., Dunlea, E. J., Aiken, A. C., Knapp, D., Weinheimer, A. J.,
508 Campos, T., Wennberg, P. O., and Jimenez, J. L.: Investigation of the sources and processing of organic aerosol
509 over the Central Mexican Plateau from aircraft measurements during MILAGRO, *Atmos. Chem. Phys.*, 10,
510 5257–5280, <https://doi.org/10.5194/acp-10-5257-2010>, 2010.
- 511 Drinovec, L., Močnik, G., Zotter, P., Prévôt, A. S. H., Ruckstuhl, C., Coz, E., Rupakheti, M., Sciare, J., Müller, T.,
512 Wiedensohler, A., and Hansen, A. D. A.: The “dual-spo” Aethalometer: an improved measurement of aerosol
513 black carbon with real-time loading compensation, *Atmos. Meas. Tech.*, 8, 1965–1979,
514 <https://doi.org/10.5194/amt-8-1965-2015>, 2015.

515 Duan, J. and Tan, J.: Atmospheric heavy metals and Arsenic in China: Situation, sources and control policies, *Atmos.*
516 *Environ.*, 74, 93–101, <https://doi.org/10.1016/j.atmosenv.2013.03.031>, 2013.

517 Elser, M., Huang, R.-J., Wolf, R., Slowik, J. G., Wang, Q.-Y., Canonaco, F., Li, G. H., Bozzetti, C., Daellenbach, K.
518 R., Huang, Y., Zhang, R.-J., Li, Z.-Q., Cao, J. J., Baltensperger, U., El-Haddad, I., and Prévôt, A. S. H.: New
519 insights into PM_{2.5} chemical composition and sources in two major cities in China during extreme haze events
520 using aerosol mass spectrometry, *Aerosols/Field Measurements/Troposphere/Chemistry (chemical composition*
521 *and reactions)*, <https://doi.org/10.5194/acpd-15-30127-2015>, 2015.

522 Ervens, B., Turpin, B. J., and Weber, R. J.: Secondary organic aerosol formation in cloud droplets and aqueous
523 particles (aqSOA): a review of laboratory, field and model studies, *Atmos. Chem. Phys.*, 11, 11069–11102,
524 <https://doi.org/10.5194/acp-11-11069-2011>, 2011.

525 Feng, T., Bei, N., Zhao, S., Wu, J. rui, Li, X., Zhang, T., Cao, J., Zhou, W., and Li, G.: Wintertime nitrate formation
526 during haze days in the Guanzhong basin, China: A case study, *Environ. Pollut.*, 243, 1057–1067,
527 <https://doi.org/10.1016/j.envpol.2018.09.069>, 2018.

528 Feng, T., Zhao, S., Zhang, X., Wang, Q., Liu, L., Li, G., and Tie, X.: Increasing wintertime ozone levels and secondary
529 aerosol formation in the Guanzhong basin, central China, *Sci. Total Environ.*, 12, 2020.

530 Feng, X., Zhang, X., He, C., and Wang, J.: Contributions of traffic and industrial emission reductions to the air quality
531 improvement after the lockdown of Wuhan and neighboring Cities due to COVID-19, *Toxics*, 9, 358,
532 <https://doi.org/10.3390/toxics9120358>, 2021.

533 Fermo, P., Artíñano, B., De Gennaro, G., Pantaleo, A. M., Parente, A., Battaglia, F., Colicino, E., Di Tanna, G.,
534 Goncalves da Silva Junior, A., Pereira, I. G., Garcia, G. S., Garcia Goncalves, L. M., Comite, V., and Miani, A.:
535 Improving indoor air quality through an air purifier able to reduce aerosol particulate matter (PM) and volatile
536 organic compounds (VOCs): Experimental results, *Environ. Pollut.*, 197, 111131,
537 <https://doi.org/10.1016/j.envres.2021.111131>, 2021.

538 Fontaras, G., Martini, G., Manfredi, U., Marotta, A., Krasenbrink, A., Maffioletti, F., Terenghi, R., and Colombo, M.:
539 Assessment of on-road emissions of four Euro V diesel and CNG waste collection trucks for supporting air-
540 quality improvement initiatives in the city of Milan, *Sci. Total Environ.*, 426, 65–72,
541 <https://doi.org/10.1016/j.scitotenv.2012.03.038>, 2012.

542 Fountoukis, C. and Nenes, A.: ISORROPIA II: a computationally efficient thermodynamic equilibrium model for
543 $K^+Ca^{2+}Mg^{2+}NH_4^+Na^+SO_4^{2-}NO_3^-Cl^-H_2O$ aerosols, *Atmos. Chem. Phys.*, 7, 4639–4659,
544 <https://doi.org/10.5194/acp-7-4639-2007>, 2007.

545 Furger, M., Rai, P., Slowik, J. G., Cao, J., Visser, S., Baltensperger, U., and Prévôt, A. S. H.: Automated alternating
546 sampling of PM₁₀ and PM_{2.5} with an online XRF spectrometer, *Atmospheric Environment: X*, 5, 100065,
547 <https://doi.org/10.1016/j.aeaoa.2020.100065>, 2020.

548

549 Gu, B., Zhang, L., Van Dingenen, R., Vieno, M., Van Grinsven, H. J., Zhang, X., Zhang, S., Chen, Y., Wang, S., Ren,
550 C., Rao, S., Holland, M., Winiwarter, W., Chen, D., Xu, J., and Sutton, M. A.: Abating ammonia is more cost-
551 effective than nitrogen oxides for mitigating PM_{2.5} air pollution, *Science*, 374, 758–762,

- 552 <https://doi.org/10.1126/science.abf8623>, 2021.
- 553 Guo, Y., Lin, C., Li, J., Wei, L., Yang, Y., Yang, Q., Li, D., Wang, H., and Shen, J.: Persistent pollution episodes,
554 transport pathways, and potential sources of air pollution during the heating season of 2016–2017 in Lanzhou,
555 China, *Environ. Monit. Assess.*, 193, 852, <https://doi.org/10.1007/s10661-021-09597-8>, 2021.
- 556 He, J., Zhao, M., Zhang, B., Wang, P., Zhang, D., Wang, M., Liu, B., Li, N., Yu, K., Zhang, Y., Zhou, T., and Jing, B.:
557 The impact of steel emissions on air quality and pollution control strategy in Caofeidian, North China, *Atmos.*
558 *Pollut. Res.*, 11, 1238–1247, <https://doi.org/10.1016/j.apr.2020.04.012>, 2020.
- 559 He, K., Huo, H., and Zhang, Q.: Urban air pollution in China: Current status, characteristics, and progress, *Annu.*
560 *Rev. Energy. Environ.*, 27, 397–431, <https://doi.org/10.1146/annurev.energy.27.122001.083421>, 2002.
- 561 Hu, W. wei, Campuzano-Jost, P., Day, D. A., Croteau, P., Canagaratna, M. R., Jayne, J. T., Worsnop, D. R., and
562 Jimenez, J. L.: Evaluation of the new capture vapourizer for aerosol mass spectrometers (AMS) through
563 laboratory studies of inorganic species, *Atmos. Meas. Tech.*, 10, 2897–2921, [https://doi.org/10.5194/amt-10-](https://doi.org/10.5194/amt-10-2897-2017)
564 [2897-2017](https://doi.org/10.5194/amt-10-2897-2017), 2017.
- 565 Huang, R.-J., He, Y., Duan, J., Li, Y., Chen, Q., Zheng, Y., Chen, Y., Hu, W., Lin, C., Ni, H., Dai, W., Cao, J., Wu, Y.,
566 Zhang, R., Xu, W., Ovadnevaite, J., Ceburnis, D., Hoffmann, T., and O’Dowd, C. D.: Contrasting sources and
567 processes of particulate species in haze days with low and high relative humidity in wintertime Beijing, *Atmos.*
568 *Chem. Phys.*, 20, 9101–9114, <https://doi.org/10.5194/acp-20-9101-2020>, 2020.
- 569 Huang, R.-J., Zhang, Y., Bozzetti, C., Ho, K.-F., Cao, J.-J., Han, Y., Daellenbach, K. R., Slowik, J. G., Platt, S. M.,
570 Canonaco, F., Zotter, P., Wolf, R., Pieber, S. M., Bruns, E. A., Crippa, M., Ciarelli, G., Piazzalunga, A.,
571 Schwikowski, M., Abbaszade, G., Schnelle-Kreis, J., Zimmermann, R., An, Z., Szidat, S., Baltensperger, U.,
572 Haddad, I. E., and Prévôt, A. S. H.: High secondary aerosol contribution to particulate pollution during haze
573 events in China, *Nature*, 514, 218–222, <https://doi.org/10.1038/nature13774>, 2014.
- 574 Huang, X., Liu, Z., Liu, J., Hu, B., Wen, T., Tang, G., Zhang, J., Wu, F. kun, Ji, D., Wang, L., and Wang, Y.: Chemical
575 characterization and source identification of PM_{2.5} at multiple sites in the Beijing–Tianjin–Hebei region, China,
576 *Atmos. Chem. Phys.*, 17, 12941–12962, <https://doi.org/10.5194/acp-17-12941-2017>, 2017.
- 577 Huang, R.-J., Wang, Y., Cao, J., Lin, C., Duan, J., Chen, Q., Li, Y., Gu, Y., Yan, J., Xu, W., Fröhlich, R., Canonaco,
578 F., Bozzetti, C., Ovadnevaite, J., Ceburnis, D., Canagaratna, M. R., Jayne, J., Worsnop, D. R., El-Haddad, I.,
579 Prévôt, A. S. H., and O’Dowd, C. D.: Primary emissions versus secondary formation of fine particulate matter
580 in the most polluted city (Shijiazhuang) in North China, *Atmos. Chem. Phys.*, 19, 2283–2298,
581 <https://doi.org/10.5194/acp-19-2283-2019>, 2019.
- 582
- 583 Huang, X., Zhang, J., Luo, B., Luo, J., Zhang, W., and Rao, Z.: Characterization of oxalic acid-containing particles
584 in summer and winter seasons in Chengdu, China, *Atmos. Environ.*, 198, 133–141,
585 <https://doi.org/10.1016/j.atmosenv.2018.10.050>, 2019.
- 586 Jin, T. sheng, Gao, J. jia, Fu, L. xin, Ai, Y., and Xu, X. H.: An evaluation of improvements in the air quality of Beijing
587 arising from the use of new vehicle emission standards, *Environ. Monit. Assess.*, 184, 2151–2159,
588 <https://doi.org/10.1007/s10661-011-2106-7>, 2012.

- 589 Khan, M. A. H., Ashfold, M. J., Nickless, G., Martin, D., Watson, L. A., Hamer, P. D., Wayne, R. P., Canosa-Mas, C.
590 E., and Shallcross, D. E.: Night-time NO₃ and OH radical concentrations in the United Kingdom inferred from
591 hydrocarbon measurements, *Atmos. Sci. Lett.*, 9, 140–146, <https://doi.org/10.1002/asl.175>, 2008.
- 592 Kuniyal, J. C. and Guleria, R. P.: The current state of aerosol-radiation interactions: A mini review, *J. Aerosol Sci.*,
593 130, 45–54, <https://doi.org/10.1016/j.jaerosci.2018.12.010>, 2019.
- 594 Kuo, C.-Y., Cheng, F.-C., Chang, S.-Y., Lin, C.-Y., Chou, C. C. K., Chou, C.-H., and Lin, Y.-R.: Analysis of the major
595 factors affecting the visibility degradation in two stations, *J. Air Waste Manage.*, 63, 433–441,
596 <https://doi.org/10.1080/10962247.2012.762813>, 2013.
- 597 Ledoux, F., Kfoury, A., Delmaire, G., Roussel, G., El Zein, A., and Courcot, D.: Contributions of local and regional
598 anthropogenic sources of metals in PM_{2.5} at an urban site in northern France, *Chemosphere*, 181, 713–724,
599 <https://doi.org/10.1016/j.chemosphere.2017.04.128>, 2017.
- 600 Lewis, C. W., Norris, G. A., Conner, T. L., and Henry, R. C.: Source apportionment of Phoenix PM_{2.5} aerosol with
601 the Unmix receptor model, *J. Air Waste Manage.*, 53, 325–338,
602 <https://doi.org/10.1080/10473289.2003.10466155>, 2003.
- 603 Li, J., Du, H., Wang, Z., Sun, Y., Yang, W., He, J., Tang, X., and Fu, P.: Rapid formation of a severe regional winter
604 haze episode over a mega-city cluster on the North China Plain, *Environ. Pollut.*, 223, 605–615,
605 <https://doi.org/10.1016/j.envpol.2017.01.063>, 2017a.
- 606
- 607 Li, J., Gao, W., Cao, L., Xiao, Y., Zhang, Y., Zhao, S., Liu, Z., Liu, Z., Tang, G., Ji, D., Hu, B., Song, T., He, L., Hu,
608 M., and Wang, Y.: Significant changes in autumn and winter aerosol composition and sources in Beijing from
609 2012 to 2018: Effects of clean air actions, *Environ. Pollut.*, 268, 115855,
610 <https://doi.org/10.1016/j.envpol.2020.115855>, 2021a.
- 611 Li, K., Zhang, X., Zhao, B., Bloss, W. J., Lin, C., White, S., Yu, H., Chen, L., Geng, C., Yang, W., Azzi, M., George,
612 C., and Bai, Z.: Suppression of anthropogenic secondary organic aerosol formation by isoprene, *npj Clim. Atmos.*
613 *Sci.*, 5, 12, <https://doi.org/10.1038/s41612-022-00233-x>, 2022.
- 614 Li, L., Tan, Q., Zhang, Y., Feng, M., Qu, Y., An, J., and Liu, X.: Characteristics and source apportionment of PM_{2.5}
615 during persistent extreme haze events in Chengdu, southwest China, *Environ. Pollut.*, 230, 718–729,
616 <https://doi.org/10.1016/j.envpol.2017.07.029>, 2017b.
- 617 Li, W., Shao, L. yi, Wang, W., Li, H., Wang, X., Li, Y., Li, W., Jones, T., and Zhang, D.: Air quality improvement in
618 response to intensified control strategies in Beijing during 2013–2019, *Sci. Total Environ.*, 744, 140776,
619 <https://doi.org/10.1016/j.scitotenv.2020.140776>, 2020.
- 620 Li, X., Bei, N., Tie, X., Wu, J., Liu, S., Wang, Q., Liu, L., Wang, R., and Li, G.: Local and transboundary transport
621 contributions to the wintertime particulate pollution in the Guanzhong Basin (GZB), China: A case study, *Sci.*
622 *Total Environ.*, 797, 148876, <https://doi.org/10.1016/j.scitotenv.2021.148876>, 2021b.
- 623 Li, Y., Sun, Y., Zhang, Q., Li, X., Li, M., Zhou, Z., and Chan, C. K.: Real-time chemical characterization of
624 atmospheric particulate matter in China: A review, *Atmos. Environ.*, 158, 270–304,

- 625 <https://doi.org/10.1016/j.atmosenv.2017.02.027>, 2017c.
- 626 Liu, J., Chen, Y., Chao, S., Cao, H., Zhang, A., Yang, Y.: Emission control priority of PM_{2.5}-bound heavy metals in
627 different seasons: A comprehensive analysis from health risk perspective, *Sci. Total Environ.*, 644, 20-30.
628 <https://doi.org/10.1016/j.scitotenv.2018.06.226>, 2018a.
- 629 Liu, B., Cheng, Y., Zhou, M., Liang, D., Dai, Q., Wang, L., Jin, W., Zhang, L., Ren, Y., Zhou, J., Dai, C., Xu, J.,
630 Wang, J., Feng, Y., and Zhang, Y.: Effectiveness evaluation of temporary emission control action in 2016 in
631 winter in Shijiazhuang, China, *Atmos. Chem. Phys.*, 18, 7019–7039, <https://doi.org/10.5194/acp-18-7019-2018>,
632 2018b.
- 633 Liu, J., Chu, B., Jia, Y., Cao, Q., Zhang, H., Chen, T., Ma, Q., Ma, J., Wang, Y., Zhang, P., and He, H.: Dramatic
634 decrease of secondary organic aerosol formation potential in Beijing: Important contribution from reduction of
635 coal combustion emission, *Sci. Total Environ.*, 832, 155045, <https://doi.org/10.1016/j.scitotenv.2022.155045>,
636 2022.
- 637 Liu, Y., Zheng, M., Yu, M., Cai, X., Du, H., Li, J., Zhou, T., Yan, C., Wang, X., Shi, Z., Harrison, R. M., Zhang, Q.,
638 and He, K.: High-time-resolution source apportionment of PM_{2.5} in Beijing with multiple models, *Atmos. Chem.*
639 *Phys.*, 19, 6595–6609, <https://doi.org/10.5194/acp-19-6595-2019>, 2019.
- 640 Liu, Z., Wang, Y., Hu, B., Ji, D., Zhang, J., Wu, F., Wan, X., and Wang, Y.: Source appointment of fine particle number
641 and volume concentration during severe haze pollution in Beijing in January 2013, *Environ. Sci. Pollut. Res.*,
642 23, 6845–6860, <https://doi.org/10.1007/s11356-015-5868-6>, 2016.
- 643
- 644 Long, X., Li, N., Tie, X., Cao, J., Zhao, S., Huang, R., Zhao, M., Li, G., and Feng, T.: Urban dust in the Guanzhong
645 Basin of China, part I: A regional distribution of dust sources retrieved using satellite data, *Sci. Total Environ.*,
646 541, 1603–1613, <https://doi.org/10.1016/j.scitotenv.2015.10.063>, 2016.
- 647 Lu, J., Ge, P., Zhao, Y.: Recent development of effect mechanism of alloying elements in titanium alloy design, *Rare*
648 *Metal Mat. Eng.*, 43, 775-779. [https://doi.org/10.1016/S1875-5372\(14\)60082-5](https://doi.org/10.1016/S1875-5372(14)60082-5), 2014.
- 649 Lu, W., Tian, Q., Xu, R., Qiu, L., Fan, Z., Wang, S., Liu, T., Huang, J., Li, Y., Wang, Y., Shi, C., Liu, Y., and Zhou,
650 Y.: Ambient air pollution and hospitalization for chronic obstructive pulmonary disease: Benefits from Three-
651 Year Action Plan, *Ecotoxicol. Environ. Saf.*, 228, 113034, <https://doi.org/10.1016/j.ecoenv.2021.113034>, 2021.
- 652 Lv, B., Zhang, B., and Bai, Y.: A systematic analysis of PM_{2.5} in Beijing and its sources from 2000 to 2012, *Atmos.*
653 *Environ.*, 124, 98–108, <https://doi.org/10.1016/j.atmosenv.2015.09.031>, 2016.
- 654 Lv, L., Chen, Y., Han, Y., Cui, M., Wei, P., Zheng, M., and Hu, J.: High-time-resolution PM_{2.5} source apportionment
655 based on multi-model with organic tracers in Beijing during haze episodes, *Sci. Total Environ.*, 772, 144766,
656 <https://doi.org/10.1016/j.scitotenv.2020.144766>, 2021.
- 657 Ma, Y., Huang, Y., Wu, J., E, J., Zhang, B., Han, D., and Ong, H. C.: A review of atmospheric fine particulate matters:
658 chemical composition, source identification and their variations in Beijing, *Energ. Source. Part A*, 44, 4783–
659 4807, <https://doi.org/10.1080/15567036.2022.2075991>, 2022.

- 660 Meng, H., Shen, Y., Fang, Y., and Zhu, Y.: Impact of the ‘Coal-to-Natural Gas’ Policy on Criteria Air Pollutants in
661 Northern China, *Atmosphere*, 13, 945, <https://doi.org/10.3390/atmos13060945>, 2022.
- 662 Meng, J., Wang, G., Li, J., Cheng, C., Ren, Y., Huang, Y., Cheng, Y., Cao, J., and Zhang, T.: Seasonal characteristics
663 of oxalic acid and related SOA in the free troposphere of Mt. Hua, central China: Implications for sources and
664 formation mechanisms, *Sci. Total Environ.*, 493, 1088–1097, <https://doi.org/10.1016/j.scitotenv.2014.04.086>,
665 2014.
- 666 Ng, N. L., Herndon, S. C., Trimborn, A., Canagaratna, M. R., Croteau, P. L., Onasch, T. B., Sueper, D., Worsnop, D.
667 R., Zhang, Q., Sun, Y. L., and Jayne, J. T.: An Aerosol Chemical Speciation Monitor (ACSM) for Routine
668 Monitoring of the Composition and Mass Concentrations of Ambient Aerosol, *Aerosol Sci. Technol.*, 45, 780–
669 794, <https://doi.org/10.1080/02786826.2011.560211>, 2011.
- 670 Ni, H., Tian, J., Wang, X., Wang, Q., Han, Y., Cao, J., Long, X., Chen, L.-W. A., Chow, J. C., Watson, J. G., Huang,
671 R.-J., and Dusek, U.: PM_{2.5} emissions and source profiles from open burning of crop residues, *Atmos. Environ.*,
672 169, 229–237, <https://doi.org/10.1016/j.atmosenv.2017.08.063>, 2017.
- 673 Ouyang, J., Song, L.-J., Ma, L.-L., Luo, M., Dai, X.-X., Zhang, J.-T., and Xu, D.-D.: Quantification of secondary
674 particle loading during a heavy air pollution event in Beijing: A simplified method based on coal emission
675 indicators, *Atmos. Environ.*, 215, 116896, <https://doi.org/10.1016/j.atmosenv.2019.116896>, 2019.
- 676 Pant, P. and Harrison, R.M.: Estimation of the contribution of road traffic emissions to particulate matter
677 concentrations from field measurements: A review, *Atmos. Environ.*, 77, 78-97.
678 <https://doi.org/10.1016/j.atmosenv.2013.04.028>, 2013.
- 679 Pang, N., Gao, J., Zhu, G., Hui, L., Zhao, P., Xu, Z., Tang, W., and Chai, F.: Impact of clean air action on the PM_{2.5}
680 pollution in Beijing, China: Insights gained from two heating seasons measurements, *Chemosphere*, 263,
681 127991, <https://doi.org/10.1016/j.chemosphere.2020.127991>, 2021.
- 682 Pöschl, U.: Atmospheric Aerosols: Composition, Transformation, Climate and Health Effects, *Angew. Chem. Int. Ed.*,
683 44, 7520–7540, <https://doi.org/10.1002/anie.200501122>, 2005.
- 684 Pui, D. Y. H., Chen, S.-C., and Zuo, Z.: PM_{2.5} in China: Measurements, sources, visibility and health effects, and
685 mitigation, *Particuology*, 13, 1–26, <https://doi.org/10.1016/j.partic.2013.11.001>, 2014.
- 686 Rai, P., Furger, M., Slowik, J. G., Canonaco, F., Fröhlich, R., Hüglin, C., Minguillón, M. C., Petterson, K.,
687 Baltensperger, U., and Prévôt, A. S. H.: Source apportionment of highly time-resolved elements during a
688 firework episode from a rural freeway site in Switzerland, *Atmos. Chem. Phys.*, 20, 1657–1674,
689 <https://doi.org/10.5194/acp-20-1657-2020>, 2020.
- 690 Ren, Y.: Chemical components and source identification of PM_{2.5} in non-heating season in Beijing: The influences
691 of biomass burning and dust, *Atmos. Res.*, 8, 2021.
- 692 Shen, G.: Changes from traditional solid fuels to clean household energies – Opportunities in emission reduction of
693 primary PM_{2.5} from residential cookstoves in China, *Biomass Bioenerg.*, 86, 28–35,
694 <https://doi.org/10.1016/j.biombioe.2016.01.004>, 2016.

- 695 Shen, W.-T., Yu, X., Zhong, S.-B., and Ge, H.-R.: Population Health Effects of Air Pollution: Fresh Evidence From
696 China Health and Retirement Longitudinal Survey, *Front. Public Health*, 9, 779552,
697 <https://doi.org/10.3389/fpubh.2021.779552>, 2021.
- 698 Shen, Z., Sun, J., Cao, J., Zhang, L., Zhang, Q., Lei, Y., Gao, J., Huang, R.-J., Liu, S., Huang, Y., Zhu, C., Xu, H.,
699 Zheng, C., Liu, P., and Xue, Z.: Chemical profiles of urban fugitive dust PM_{2.5} samples in Northern Chinese
700 cities, *Sci. Total Environ.*, 569–570, 619–626, <https://doi.org/10.1016/j.scitotenv.2016.06.156>, 2016.
- 701 Simka, H., Shankar, S., Duran, C., and Haverty, M.: Fundamentals of Cu/Barrier-Layer Adhesion in Microelectronic
702 Processing, *MRS Proc.*, 863, B9.2, <https://doi.org/10.1557/PROC-863-B9.2>, 2005.
- 703 Tao, J., Zhang, L., Cao, J., and Zhang, R.: A review of current knowledge concerning PM_{2.5} chemical composition,
704 aerosol optical properties and their relationships across China, *Atmos. Chem. Phys.*, 17, 9485–9518,
705 <https://doi.org/10.5194/acp-17-9485-2017>, 2017. Tao, J., Zhang, L., Zhang, Z., Huang, R., Wu, Y., Zhang, R.,
706 Cao, J., and Zhang, Y.: Control of PM_{2.5} in Guangzhou during the 16th Asian Games period: Implication for
707 hazy weather prevention, *Sci. Total Environ.*, 508, 57–66, <https://doi.org/10.1016/j.scitotenv.2014.11.074>, 2015.
- 708 Tao, Y., Ye, X., Ma, Z., Xie, Y., Wang, R., Chen, J., Yang, X., and Jiang, S.: Insights into different nitrate formation
709 mechanisms from seasonal variations of secondary inorganic aerosols in Shanghai, *Atmos. Environ.*, 145, 1–9,
710 <https://doi.org/10.1016/j.atmosenv.2016.09.012>, 2016.
- 711 Thorpe, A. and Harrison, R. M.: Sources and properties of non-exhaust particulate matter from road traffic: A review,
712 *Sci. Total Environ.*, 400, 270–282, <https://doi.org/10.1016/j.scitotenv.2008.06.007>, 2008.
- 713 Tian, H. Z., Lu, L., Hao, J. M., Gao, J. J., Cheng, K., Liu, K. Y., Qiu, P. P., and Zhu, C. Y.: A Review of key hazardous
714 trace elements in Chinese coals: Abundance, occurrence, behavior during coal combustion and their
715 environmental impacts, *Energ. Fuel.*, 27, 601–614, <https://doi.org/10.1021/ef3017305>, 2013.
- 716 Tian, J., Wang, Q., Zhang, Y., Yan, M., Liu, H., Zhang, N., Ran, W., and Cao, J.: Impacts of primary emissions and
717 secondary aerosol formation on air pollution in an urban area of China during the COVID-19 lockdown, *Environ.*
718 *Int.*, 150, 106426, <https://doi.org/10.1016/j.envint.2021.106426>, 2021.
- 719 Tian, J., Wang, Q., Liu, H., Ma, Y., Liu, S., Zhang, Y., Ran, W., Han, Y., and Cao, J.: Measurement report: The
720 importance of biomass burning in light extinction and direct radiative effect of urban aerosol during the COVID-
721 19 lockdown in Xi'an, China, *Atmos. Chem. Phys.*, 22, 8369–8384, <https://doi.org/10.5194/acp-22-8369-2022>,
722 2022.
- 723 Tian, Y. Z., Wang, J., Peng, X., Shi, G. L., and Feng, Y. C.: Estimation of the direct and indirect impacts of fireworks
724 on the physicochemical characteristics of atmospheric PM₁₀ and PM_{2.5}, *Atmos. Chem. Phys.*, 14, 9469–9479,
725 <https://doi.org/10.5194/acp-14-9469-2014>, 2014.
- 726 Vu, T. V., Shi, Z., Cheng, J., Zhang, Q., He, K., Wang, S., and Harrison, R. M.: Assessing the impact of clean air
727 action on air quality trends in Beijing using a machine learning technique, *Atmos. Chem. Phys.*, 19, 11303–
728 11314, <https://doi.org/10.5194/acp-19-11303-2019>, 2019.
- 729 Wang, C., Li, X., Zhang, T., Tang, A., Cui, M., Liu, X., Ma, X., Zhang, Y., Liu, X., and Zheng, M.: Developing
730 Nitrogen Isotopic Source Profiles of Atmospheric Ammonia for Source Apportionment of Ammonia in Urban

- 731 Beijing, *Front. Environ. Sci.*, 10, 903013, <https://doi.org/10.3389/fenvs.2022.903013>, 2022a.
- 732 Wang, F., Yu, H., Wang, Z., Liang, W., Shi, G., Gao, J., Li, M., and Feng, Y.: Review of online source apportionment
733 research based on observation for ambient particulate matter, *Sci. Total Environ.*, 762, 144095,
734 <https://doi.org/10.1016/j.scitotenv.2020.144095>, 2021a.
- 735 Wang, H. and Zhao, L.: A joint prevention and control mechanism for air pollution in the Beijing-Tianjin-Hebei
736 region in china based on long-term and massive data mining of pollutant concentration, *Atmos. Environ.*, 174,
737 25–42, <https://doi.org/10.1016/j.atmosenv.2017.11.027>, 2018.
- 738 Wang, J., Zhao, B., Wang, S., Yang, F., Xing, J., Morawska, L., Ding, A., Kulmala, M., Kerminen, V.-M., Kujansuu,
739 J., Wang, Z., Ding, D., Zhang, X., Wang, H., Tian, M., Petäjä, T., Jiang, J., and Hao, J.: Particulate matter
740 pollution over China and the effects of control policies, *Sci. Total Environ.*, 584–585, 426–447,
741 <https://doi.org/10.1016/j.scitotenv.2017.01.027>, 2017.
- 742 Wang, L., Wang, X., Gu, R., Wang, H., Yao, L., Wen, L., Zhu, F., Wang, W., Xue, L., Yang, L., Lu, K., Chen, J., Wang,
743 T., Zhang, Y., and Wang, W.: Observations of fine particulate nitrated phenols in four sites in northern China:
744 concentrations, source apportionment, and secondary formation, *Atmos. Chem. Phys.*, 18, 4349–4359,
745 <https://doi.org/10.5194/acp-18-4349-2018>, 2018.
- 746 Wang, L. T., Wei, Z., Yang, J., Zhang, Y., Zhang, F. F., Su, J., Meng, C. C., and Zhang, Q.: The 2013 severe haze over
747 southern Hebei, China: model evaluation, source apportionment, and policy implications, *Atmos. Chem. Phys.*,
748 14, 3151–3173, <https://doi.org/10.5194/acp-14-3151-2014>, 2014.
- 749 Wang, M., Tian, P., Wang, L., Yu, Z., Du, T., Chen, Q., Guan, X., Guo, Y., Zhang, M., Tang, C., Chang, Y., Shi, J.,
750 Liang, J., Cao, X., and Zhang, L.: High contribution of vehicle emissions to fine particulate pollutions in
751 Lanzhou, Northwest China based on high-resolution online data source appointment, *Sci. Total Environ.*, 798,
752 149310, <https://doi.org/10.1016/j.scitotenv.2021.149310>, 2021b.
- 753 Wang, P., Cao, J., Shen, Z., Han, Y., Lee, S., Huang, Y., Zhu, C., Wang, Q., Xu, H., and Huang, R.: Spatial and
754 seasonal variations of PM_{2.5} mass and species during 2010 in Xi'an, China, *Sci. Total Environ.*, 508, 477–487,
755 <https://doi.org/10.1016/j.scitotenv.2014.11.007>, 2015.
- 756 Wang, Q., Ye, J., Wang, Y., Zhang, T., Ran, W., Wu, Y., Tian, J., Li, L., Zhou, Y., Hang Ho, S. S., Dang, B., Zhang,
757 Q., Zhang, R., Chen, Y., Zhu, C., and Cao, J.: Wintertime Optical Properties of Primary and Secondary Brown
758 Carbon at a Regional Site in the North China Plain, *Environ. Sci. Technol.*, 53, 12389–12397,
759 <https://doi.org/10.1021/acs.est.9b03406>, 2019.
- 760 Wang, Y., Wang, Q., Ye, J., Yan, M., Qin, Q., Prévôt, A. S. H., and Cao, J.: A Review of Aerosol Chemical
761 Composition and Sources in Representative Regions of China during Wintertime, *Atmosphere*, 10, 277,
762 <https://doi.org/10.3390/atmos10050277>, 2019.
- 763 Wang, Y., Zhang, Q. Q., He, K., Zhang, Q., and Chai, L.: Sulfate-nitrate-ammonium aerosols over China: response
764 to 2000–2015 emission changes of sulfur dioxide, nitrogen oxides, and ammonia, *Atmos. Chem. Phys.*, 13,
765 2635–2652, <https://doi.org/10.5194/acp-13-2635-2013>, 2013.
- 766 Wang, Y., Yuan, Y., Wang, Q., Liu, C., Zhi, Q., and Cao, J.: Changes in air quality related to the control of coronavirus

- 767 in China: Implications for traffic and industrial emissions, *Sci. Total Environ.*, 731, 139133,
768 <https://doi.org/10.1016/j.scitotenv.2020.139133>, 2020a.
- 769 Wang, Y., Yu, M., Wang, Y., Tang, G., Song, T., Zhou, P., Liu, Z., Hu, B., Ji, D., Wang, L., Zhu, X., Yan, C., Ehn, M.,
770 Gao, W., Pan, Y., Xin, J., Sun, Y., Kerminen, V.-M., Kulmala, M., and Petäjä, T.: Rapid formation of intense
771 haze episodes via aerosol–boundary layer feedback in Beijing, *Atmos. Chem. Phys.*, 20, 45–53,
772 <https://doi.org/10.5194/acp-20-45-2020>, 2020b.
- 773 Wang, Y., Liu, C., Wang, Q., Qin, Q., Ren, H., and Cao, J.: Impacts of natural and socioeconomic factors on PM_{2.5}
774 from 2014 to 2017, *J. Environ. Manage.*, 284, 112071, <https://doi.org/10.1016/j.jenvman.2021.112071>, 2021c.
- 775 Wang, Z., Wang, R., Wang, J., Wang, Y., McPherson Donahue, N., Tang, R., Dong, Z., Li, X., Wang, L., Han, Y., and
776 Cao, J.: The seasonal variation, characteristics and secondary generation of PM_{2.5} in Xi’an, China, especially
777 during pollution events, *Environ. Res.*, 212, 113388, <https://doi.org/10.1016/j.envres.2022.113388>, 2022b.
- 778 Wei, F., Yang G., Jiang, D., Liu, Z., Sun, B.: Basic statistics and characteristics of background values of soil elements
779 in China. *Environ. Monit. in China (in Chinese)* 7, 1–6. <https://doi.org/10.19316/j.issn.1002-6002.1991.01.001>,
780 1991.
- 781 Wood, E. C., Canagaratna, M. R., Herndon, S. C., Onasch, T. B., Kolb, C. E., Worsnop, D. R., Kroll, J. H., Knighton,
782 W. B., Seila, R., Zavala, M., Molina, L. T., DeCarlo, P. F., Jimenez, J. L., Weinheimer, A. J., Knapp, D. J., Jobson,
783 B. T., Stutz, J., Kuster, W. C., and Williams, E. J.: Investigation of the correlation between odd oxygen and
784 secondary organic aerosol in Mexico City and Houston, *Atmos. Chem. Phys.*, 10, 8947–8968,
785 <https://doi.org/10.5194/acp-10-8947-2010>, 2010.
- 786 Xu, H. M., Cao, J. J., Ho, K. F., Ding, H., Han, Y. M., Wang, G. H., Chow, J. C., Watson, J. G., Khol, S. D., Qiang,
787 J., and Li, W. T.: Lead concentrations in fine particulate matter after the phasing out of leaded gasoline in Xi’an,
788 China, *Atmos. Environ.*, 46, 217–224, <https://doi.org/10.1016/j.atmosenv.2011.09.078>, 2012.
- 789 Xu, J., Liu, D., Wu, X., Vu, T. V., Zhang, Y., Fu, P., Sun, Y., Xu, W., Zheng, B., Harrison, R. M., and Shi, Z.: Source
790 apportionment of fine organic carbon at an urban site of Beijing using a chemical mass balance model, *Atmos.*
791 *Chem. Phys.*, 21, 2021.
- 792 Xu, P., Yang, Y., Zhang, J., Gao, W., Liu, Z., Hu, B., and Wang, Y.: Characterization and source identification of
793 submicron aerosol during serious haze pollution periods in Beijing, *J. of Environ. Sci.*, 112, 25–37,
794 <https://doi.org/10.1016/j.jes.2021.04.005>, 2022.
- 795 Xu, W., Croteau, P., Williams, L., Canagaratna, M., Onasch, T., Cross, E., Zhang, X., Robinson, W., Worsnop, D.,
796 and Jayne, J.: Laboratory characterization of an aerosol chemical speciation monitor with PM_{2.5} measurement
797 capability, *Aerosol Sci. Technol.*, 51, 69–83, <https://doi.org/10.1080/02786826.2016.1241859>, 2017.
- 798 Xue, J., Griffith, S. M., Yu, X., Lau, A. K. H., and Yu, J. Z.: Effect of nitrate and sulfate relative abundance in PM_{2.5}
799 on liquid water content explored through half-hourly observations of inorganic soluble aerosols at a polluted
800 receptor site, *Atmos. Environ.*, 99, 24–31, <https://doi.org/10.1016/j.atmosenv.2014.09.049>, 2014.
- 801 Yan, Y., Sun, Y. B., Weiss, D., Liang, L. J., and Chen, H. Y.: Polluted dust derived from long-range transport as a
802 major end member of urban aerosols and its implication of non-point pollution in northern China, *Sci. Total*

803 Environ., 506–507, 538–545, <https://doi.org/10.1016/j.scitotenv.2014.11.071>, 2015.

804 Yang, D., Li, Z., Yue, Z., Liu, J. X., Zhai, Z., Li, Z., Gao, M., Hu, A. L., Zhu, W. J., Ding, N., Li, Z., Guo, S., Wang,
805 X., Wang, L., and Wei, J.: Variations in sources, composition, and exposure risks of PM_{2.5} in both pre-heating
806 and heating seasons, *Aerosol Air Qual. Res.*, 22, 14, <https://doi.org/10.4209/aaqr.210333>, 2022a.

807 Yang, S., Yuan, B., Peng, Y., Huang, S., Chen, W., Hu, W., Pei, C., Zhou, J., Parrish, D. D., Wang, W., He, X., Cheng,
808 C., Li, X.-B., Yang, X., Song, Y., Wang, H., Qi, J., Wang, B., Wang, C., Wang, C., Wang, Z., Li, T., Zheng, E.,
809 Wang, S., Wu, C., Cai, M., Ye, C., Song, W., Cheng, P., Chen, D., Wang, X., Zhang, Z., Wang, X., Zheng, J.,
810 and Shao, M.: The formation and mitigation of nitrate pollution: comparison between urban and suburban
811 environments, *Atmos. Chem. Phys.*, 22, 4539–4556, <https://doi.org/10.5194/acp-22-4539-2022>, 2022b.

812 Yang, X. and Teng, F.: The air quality co-benefit of coal control strategy in China, *Resour. Conserv. Recy.*, 129, 373–
813 382, <https://doi.org/10.1016/j.resconrec.2016.08.011>, 2018.

814 Yang, X., Zheng, M., Liu, Y., Yan, C., Liu, J., Liu, J., and Cheng, Y.: Exploring sources and health risks of metals in
815 Beijing PM_{2.5}: Insights from long-term online measurements, *Sci. Total Environ.*, 814, 151954,
816 <https://doi.org/10.1016/j.scitotenv.2021.151954>, 2022c.

817 Zeng, J. and He, Q.: Does industrial air pollution drive health care expenditures? Spatial evidence from China, *J.*
818 *Clean. Prod.*, 218, 400–408, <https://doi.org/10.1016/j.jclepro.2019.01.288>, 2019.

819 Zhang, Q., Zheng, Y., Tong, D., Shao, M., Wang, S., Zhang, Y., Xu, X., Wang, J., He, H., Liu, W., Ding, Y., Lei, Y.,
820 Li, J., Wang, Z., Zhang, X., Wang, Y., Cheng, J., Liu, Y., Shi, Q., Yan, L., Geng, G., Hong, C., Li, M., Liu, F.,
821 Zheng, B., Cao, J., Ding, A., Gao, J., Fu, Q., Huo, J., Liu, B., Liu, Z., Yang, F., He, K., and Hao, J.: Drivers of
822 improved PM_{2.5} air quality in China from 2013 to 2017, *Proc. Natl. Acad. Sci. U.S.A.*, 116, 24463–24469,
823 <https://doi.org/10.1073/pnas.1907956116>, 2019.

824 Zhang, Y., Vu, T. V., Sun, J., He, J., Shen, X., Lin, W., Zhang, X., Zhong, J., Gao, W., Wang, Y., Fu, T. M., Ma, Y., Li,
825 W., and Shi, Z.: Significant changes in chemistry of fine particles in wintertime Beijing from 2007 to 2017:
826 Impact of Clean Air Actions, *Environ. Sci. Technol.*, 54, 1344–1352, <https://doi.org/10.1021/acs.est.9b04678>,
827 2020.

828 Zhang, Z., Gao, J., Zhang, L., Wang, H., Tao, J., Qiu, X., Chai, F., Li, Y., and Wang, S.: Observations of biomass
829 burning tracers in PM_{2.5} at two megacities in North China during 2014 APEC summit, *Atmos. Environ.*, 169,
830 54–64, <https://doi.org/10.1016/j.atmosenv.2017.09.011>, 2017.

831 Zhao, P., Feng, Y., Zhu, T., and Wu, J.: Characterizations of resuspended dust in six cities of North China, *Atmos.*
832 *Environ.*, 40, 5807–5814, <https://doi.org/10.1016/j.atmosenv.2006.05.026>, 2006.

833 Zhao, S., Tian, H., Luo, L., Liu, H., Wu, B., Liu, S., Bai, X., Liu, W., Liu, X., Wu, Y., Lin, S., Guo, Z., Lv, Y., and
834 Xue, Y.: Temporal variation characteristics and source apportionment of metal elements in PM_{2.5} in urban
835 Beijing during 2018–2019, *Environ. Pollut.*, 268, 115856, <https://doi.org/10.1016/j.envpol.2020.115856>, 2021.

836 Zheng, G., Duan, F., Ma, Y., Zhang, Q., Huang, T., Kimoto, T., Cheng, Y., Su, H., and He, K.: Episode-Based
837 Evolution Pattern Analysis of Haze Pollution: Method Development and Results from Beijing, China, *Environ.*
838 *Sci. Technol.*, 50, 4632–4641, <https://doi.org/10.1021/acs.est.5b05593>, 2016.

- 839 Zhang, R., Jing, J., Tao, J., Hsu, S.-C., Wang, G., Cao, J., Lee, C. S. L., Zhu, L., Chen, Z., Zhao, Y., and Shen, Z.:
840 Chemical characterization and source apportionment of PM_{2.5} in Beijing: seasonal perspective, *Atmos. Chem.*
841 *Phys.*, 13, 7053–7074, <https://doi.org/10.5194/acp-13-7053-2013>, 2013.
- 842 Zheng, M., Wang, Y., Yuan, L., Chen, N., and Kong, S.: Ambient observations indicating an increasing effectiveness
843 of ammonia control in wintertime PM_{2.5} reduction in Central China, *Sci. Total Environ.*, 824, 153708,
844 <https://doi.org/10.1016/j.scitotenv.2022.153708>, 2022.
- 845 Zhou, W., Lei, L., Du, A., Zhang, Z., Li, Y., Yang, Y., Tang, G., Chen, C., Xu, W., Sun, J., Li, Z., Fu, P., Wang, Z.,
846 and Sun, Y.: Unexpected increases of severe haze pollution during the post COVID - 19 Period: Effects of
847 emissions, meteorology, and secondary production, *J. Geophys. Res-Atmos.*, 127,
848 <https://doi.org/10.1029/2021JD035710>, 2022.
- 849 Ziemann, P. J. and Atkinson, R.: Kinetics, products, and mechanisms of secondary organic aerosol formation, *Chem.*
850 *Soc. Rev.*, 41, 6582, <https://doi.org/10.1039/c2cs35122f>, 2012.
- 851

852 **Table 1.** Meteorological conditions, gas pollutants, chemical composition, and source contribution of PM_{2.5} during
 853 pollution episodes in Xi'an, Shijiazhuang, and Beijing

Parameters	Xi'an		Shijiazhuang			Beijing		
	EP1	EP2	EP3	EP4	EP5	EP6	EP7	EP8
T (°C)	4.9 ± 2.6	1.5 ± 3.5	0.4 ± 3.4	-0.2 ± 3.3	-2.7 ± 3.3	0.3 ± 3.2	-1.6 ± 3.3	5.1 ± 3.6
RH (%)	52 ± 10	45 ± 10	61 ± 15	40 ± 13	75 ± 11	57 ± 19	45 ± 24	36 ± 10
WS (m s ⁻¹)	0.5 ± 0.2	0.7 ± 0.3	1.4 ± 0.6	1.9 ± 0.8	1.4 ± 0.7	1.0 ± 0.6	1.1 ± 0.6	1.0 ± 0.6
Dominant WD ^a	WSW, WNW	WSW	NNW	NNW	NNW	NNE	NNW, NNE	NNE, ENE
CO (mg m ⁻³)	1.39 ± 0.40	1.15 ± 0.56	1.47 ± 0.62	0.60 ± 0.30	0.43 ± 0.33	1.04 ± 0.56	0.81 ± 0.32	1.00 ± 0.55
SO ₂ (µg m ⁻³)	15 ± 3	15 ± 5	9 ± 4	8 ± 4	3 ± 1	6 ± 5	4 ± 3	6 ± 4
NO ₂ (µg m ⁻³)	74 ± 22	63 ± 32	63 ± 14	47 ± 21	27 ± 11	54 ± 22	46 ± 17	42 ± 21
O ₃ (ppm)	47 ± 8	42 ± 10	36 ± 7	32 ± 6	27 ± 3	36 ± 6	33 ± 4	43 ± 9
ALWC (µg m ⁻³)	15 ± 11	8 ± 8	42 ± 37	12 ± 11	59 ± 448	28 ± 47	23 ± 8	11 ± 13
Dominant Chemical composition	OA (38%) NO ₃ ⁻ (24%)	OA (34%) NO ₃ ⁻ (24%)	NO ₃ ⁻ (27%) OA (26%)	OA (30%) NO ₃ ⁻ (23%)	NO ₃ ⁻ (32%) OA (26%)	OA (32%) NO ₃ ⁻ (26%)	OA (32%) NO ₃ ⁻ (26%)	OA (40%) NO ₃ ⁻ (23%)
Dominant source contribution ^b	BB (30%) SF (25%) CC (17%)	SF (34%) BB (24%) VE (16%)	SF (39%) BB (23%) CC (16%)	BB (40%) CC (16%) VE (16%)	SF (70%) BB (16%)	SF (62%) BB (13%)	SF (61%) BB (14%)	BB (38%) SF (27%) VE (15%)

854 ^a WSW: west-southwest; WNW: west-northwest; NNW: north-northwest; NNE: north-northeast; ENE: East-northeast

855 ^b BB: biomass burning; SF: secondary formation source; CC: coal combustion; VE: vehicle emission

856

857 **Figure captions:**

858 **Figure 1.** Chemical composition and source apportionment results of PM_{2.5} in three pilot cities of northern China
859 during the sampling period.

860 **Figure 2.** Mass fractions of chemical components (a-c) and sources contribution (d-f) with reconstructed PM_{2.5}
861 concentration in Xi'an, Shijiazhuang, and Beijing.

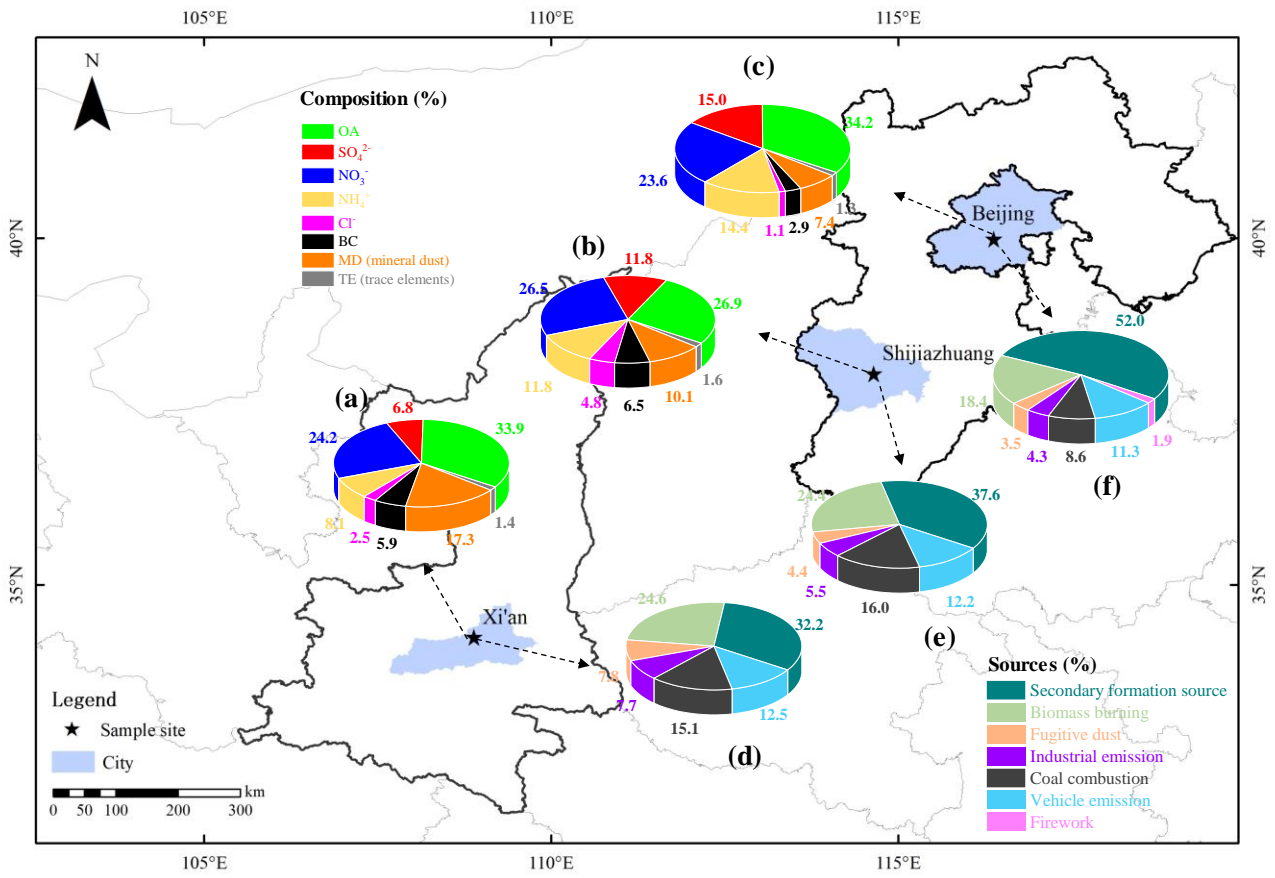
862 **Figure 3.** Correlations of secondary formation source/ Δ CO and O_x mixing ratio in (a) Xi'an, (b) Shijiazhuang, and
863 (c) Beijing. Each point and its error bar represent the mean and standard deviation in each bin (Δ O_x = 5 ppb).

864 **Figure 4.** Correlation of secondary formation source/ Δ CO and ALWC during sampling periods in (a) Xi'an, (b)
865 Shijiazhuang, and (c) Beijing, respectively. The points and error bar represent the mean values and standard deviation
866 values of secondary formation source/ Δ CO and ALWC in each bin. In Xi'an, each bin is 5 $\mu\text{g m}^{-3}$ (Δ ALWC = 5 μg
867 m^{-3}). In Shijiazhuang, each bin is 5 $\mu\text{g m}^{-3}$ (Δ ALWC = 5 $\mu\text{g m}^{-3}$) when ALWC ranged from 0 to 75 $\mu\text{g m}^{-3}$, but 25 μg
868 m^{-3} (Δ ALWC = 25 $\mu\text{g m}^{-3}$) for ALWC ranged from 75 to 200 $\mu\text{g m}^{-3}$ due to limitations in data. In Beijing, each bin
869 is 5 $\mu\text{g m}^{-3}$ (Δ ALWC = 5 $\mu\text{g m}^{-3}$) when ALWC ranged from 0 to 50 $\mu\text{g m}^{-3}$, but 100 $\mu\text{g m}^{-3}$ (Δ ALWC = 100 $\mu\text{g m}^{-3}$)
870 for ALWC ranged from 50 to 900 $\mu\text{g m}^{-3}$ due to limitations in data.

871 **Figure 5.** Summary of PM_{2.5} and its composition (a, b, c) and source contribution (d, e, f) in Xi'an, Shijiazhuang,
872 and Beijing in winter in past decades. Where * represents the result of this study. The data and references used for
873 this figure are listed in Table S5 and S7.

874

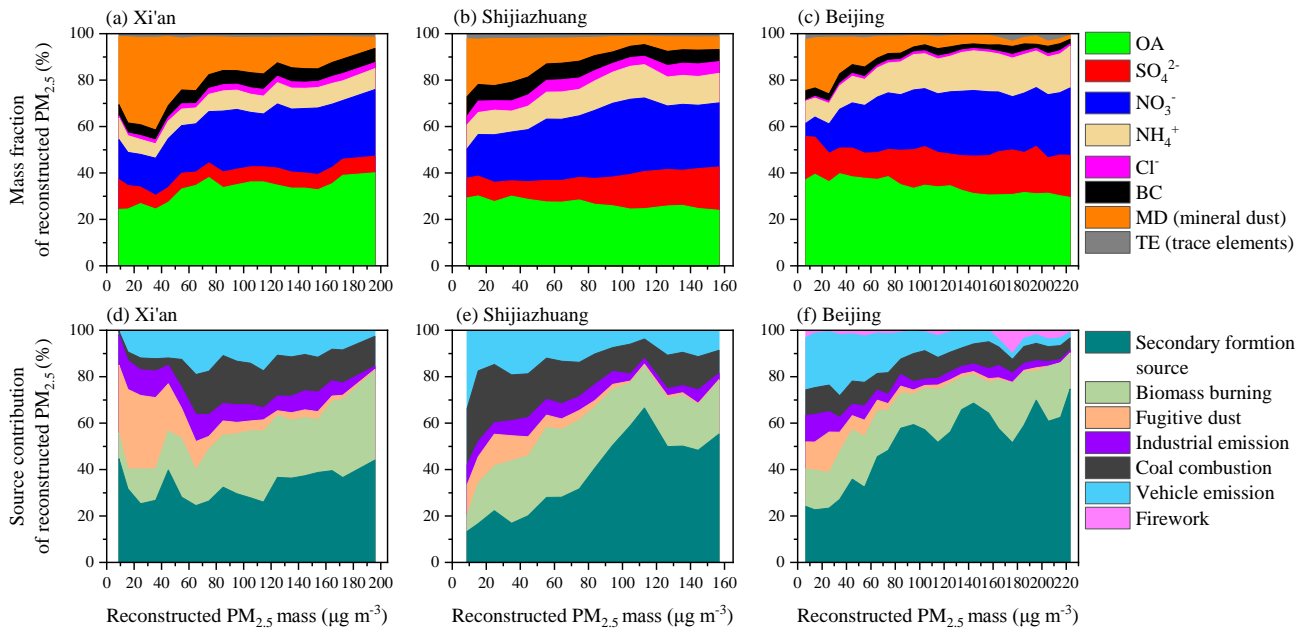
875



876

877 **Figure 1.** Chemical composition and source apportionment results of PM_{2.5} in three pilot cities of northern China
 878 during the sampling period.

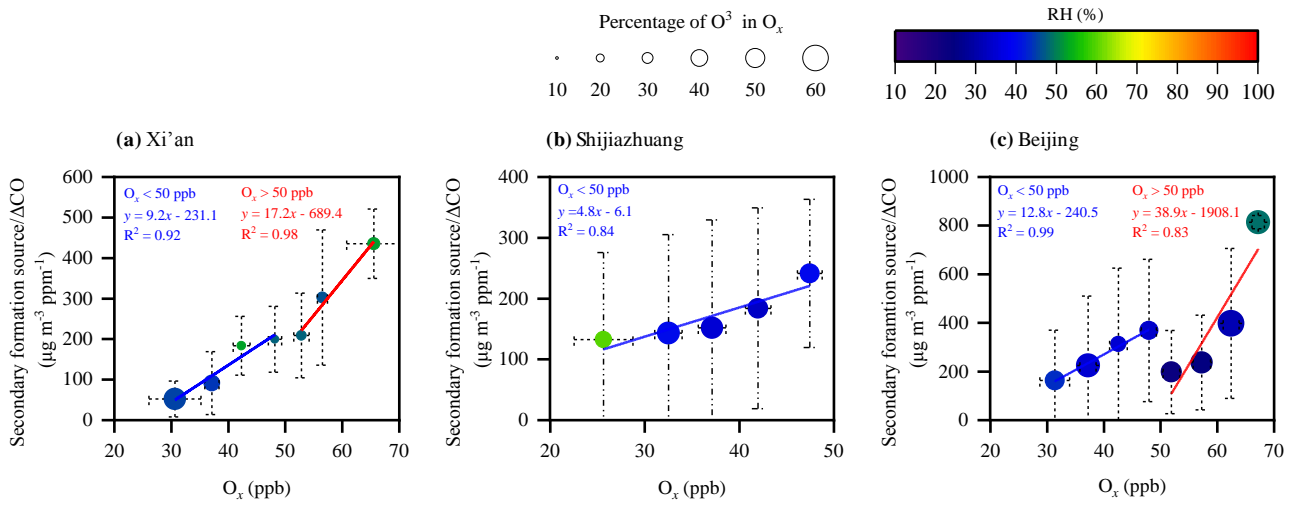
879



881

882 **Figure 2.** Mass fractions of chemical components (a-c) and sources contribution (d-f) with reconstructed $PM_{2.5}$
 883 concentration in Xi'an, Shijiazhuang, and Beijing.

884

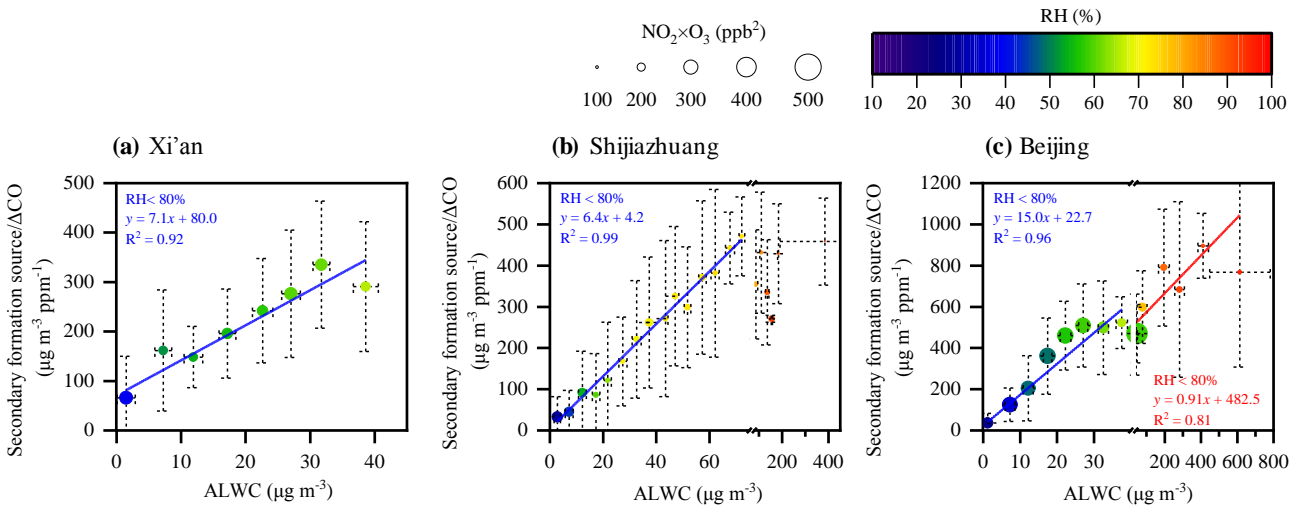


886

887 **Figure 3.** Correlations of secondary formation source/ΔCO and O_x mixing ratio in (a) Xi'an, (b) Shijiazhuang, and
 888 (c) Beijing. Each point and its error bar represent the mean and standard deviation in each bin ($\Delta\text{O}_x = 5$ ppb).

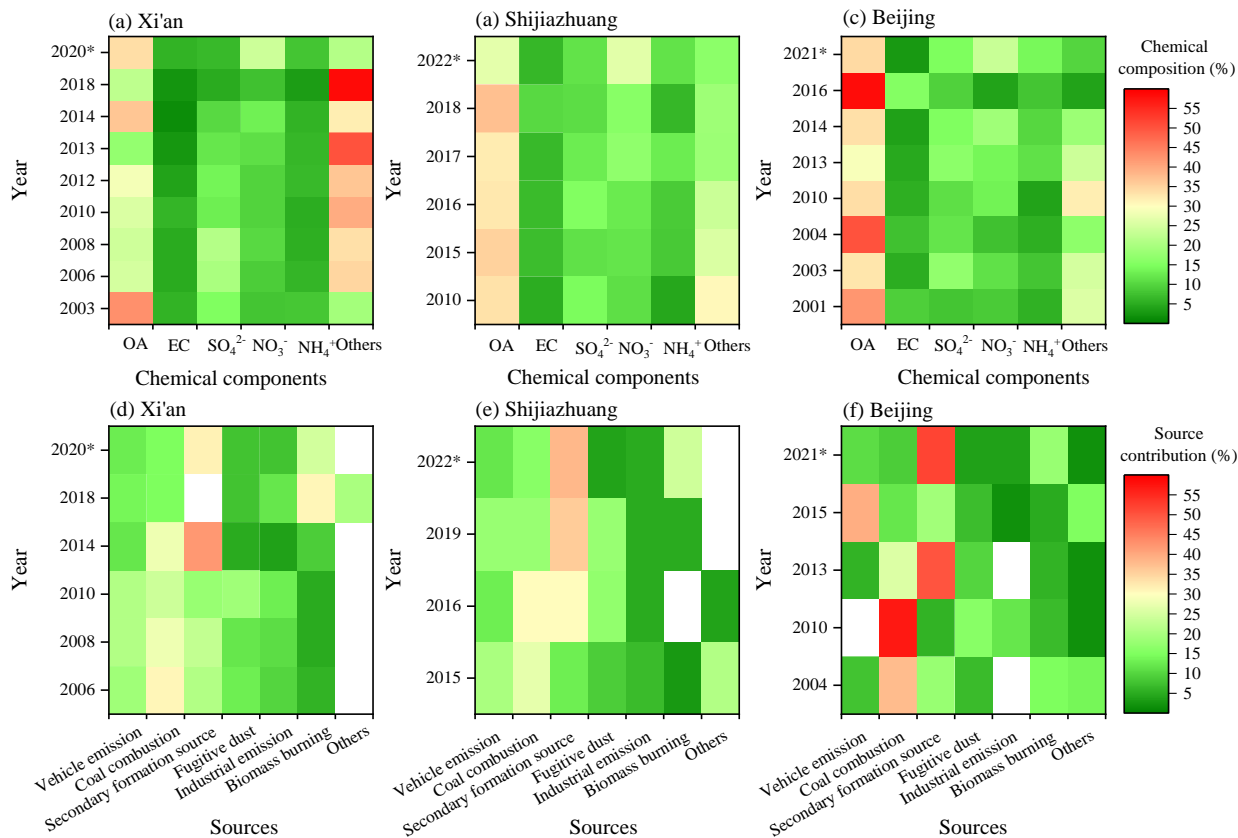
889

890



891

892 **Figure 4.** Correlation of secondary formation source/ΔCO and ALWC during sampling periods in (a) Xi'an, (b)
 893 Shijiazhuang, and (c) Beijing, respectively. The points and error bar represent the mean values and standard deviation
 894 values of secondary formation source/ΔCO and ALWC in each bin. In Xi'an, each bin is $5 \mu\text{g m}^{-3}$ ($\Delta\text{ALWC} = 5 \mu\text{g m}^{-3}$).
 895 m^{-3}). In Shijiazhuang, each bin is $5 \mu\text{g m}^{-3}$ ($\Delta\text{ALWC} = 5 \mu\text{g m}^{-3}$) when ALWC ranged from 0 to $75 \mu\text{g m}^{-3}$, but $25 \mu\text{g m}^{-3}$
 896 m^{-3} ($\Delta\text{ALWC} = 25 \mu\text{g m}^{-3}$) for ALWC ranged from 75 to $200 \mu\text{g m}^{-3}$ due to limitations in data. In Beijing, each bin
 897 is $5 \mu\text{g m}^{-3}$ ($\Delta\text{ALWC} = 5 \mu\text{g m}^{-3}$) when ALWC ranged from 0 to $50 \mu\text{g m}^{-3}$, but $100 \mu\text{g m}^{-3}$ ($\Delta\text{ALWC} = 100 \mu\text{g m}^{-3}$)
 898 for ALWC ranged from 50 to $900 \mu\text{g m}^{-3}$ due to limitations in data.



899

900 **Figure 5.** Summary of PM_{2.5} and its composition (a, b, c) and source contribution (d, e, f) in Xi'an, Shijiazhuang,
 901 and Beijing in winter in past decades. Where * represents the result of this study, and the empty white area means no
 902 data. The data and references used for this figure are listed in Table S7 and S8.

903